



國立臺灣大學工學院化學工程學系

碩士論文

Department of Chemical Engineering

College of Engineering

National Taiwan University

Master Thesis

磷脂質輔助合成含鎂氫氧基磷灰石應用於骨修復材料

Lipid-Assisted Synthesis of Magnesium-Loaded
Hydroxyapatite for Bone Healing

陳妤欣

Yu-Hsin Chen

指導教授：吳嘉文 博士

Advisor: Kevin C.-W. Wu, Ph.D.

中華民國 108 年 6 月

June 2019

誌謝



轉眼間兩年的碩士生涯即將邁入尾聲，首先感謝指導教授吳嘉文老師當初願意收我當您的學生，加入 WuLab 這個大家庭，謝謝您的栽培與指導，讓我在生醫材料的領域上沒有迷失方向，總是能引導並指正我往正確的方向前進，透過每次的進度討論訓練我在邏輯思考及分析整合的能力，也因為老師的鼓勵與協助，可以參加許多國內外的研討會，還記得老師在我心情不好的時候關心我的心情狀況，覺得很窩心，非常謝謝老師這兩年來的照顧！另外，特別感謝口試委員們，林峰輝、方旭偉、張瑛芝、胡晉嘉教授給予我許多的指導與建議，使此論文更加完整。

接著謝謝我的夥伴們，感謝生醫組的好戰友，宏霖，處理生醫組的大小事，教我許多細胞培養的細節並抽空跟我討論實驗，在養細胞養到崩潰的時候可以互相鼓勵。感謝襄伶在實驗室時常幫助我解決許多事情，在最後口試的時候幫忙修改簡報並且給我中肯的建議。感謝靖柔在修課的時候都會提醒我要交作業、準備考試。特別感謝俊毅學長，在材料鑑定上給了很多協助與建議，也幫忙修改論文文法，讓內容更加順暢。感謝寶韜在研究上給予指導並協助，帶領我研究含鎂磷酸鈣材料。謝謝生醫組學弟祐陞，幫忙處理細胞房的雜事及研究計畫的撰寫。感謝實驗室的學長姐 Chi、偉琪、正彥、澄惠、希彥、哲維、祐德、韓柏、任軒、babasaheb 曾在研究上的幫助，也感謝學弟妹瑋呈、嘉軒、晏慈、益承、怡婷帶給實驗室許多歡樂。

感謝我的好朋友湘宜，在無數個夜晚不睡覺陪我聊天，也時常在假日北上陪我購物紓壓，也謝謝子喬、亞茹這兩年在台大的陪伴。感謝我的室友佳樺在準備口試期間經常熬夜聽我練習。最後感謝一直以來支持我的家人，讓我可以無後顧之憂的環境下完成碩士論文。

Abstract



Magnesium-loaded hydroxyapatite (Mg@HAp) is a potential biomaterial for bone healing application but has not been comprehensively synthesized yet. In this study, we utilize a phosphatidylcholine (PC)-assisted method for synthesizing Mg@HAp with controllable Mg amount from 1.44 to 10.64 wt%. It is proposed that the negatively charged phosphate functional group of PC could act on cations (i.e. Mg^{2+} or Ca^{2+}), which provides a stable nucleation for the formation of Mg@HAp. We optimize synthetic conditions for achieving a Mg@HAp with a relatively low crystallinity which is similar to human bone structure, as evidenced by XRD measurement. The *in vitro* test of bone cells (MG63) shows that the release of Mg^{2+} ions from Mg@HAp enhances cellular proliferation and differentiation. We believe the synthesized Mg@HAp would be a promising biomaterial in orthopedic applications.

Keywords: hydroxyapatite, magnesium, phosphatidylcholine, bone healing, MG63 osteoblast-like cells.

摘要



含鎂氫氧基磷灰石應用於骨修復填補材料具有極大的發展潛力，但高鎂含量的氫氧基磷灰石之合成方法仍尚未發展成熟。在這項研究中，我們利用磷脂質(磷脂酰膽鹼)輔助合成含鎂氫氧基磷灰石，其中，鎂在材料中的重量百分比可控制在 1.44 至 10.64 % 之間。利用磷脂質中帶負電荷的磷酸官能基可作用於陽離子(如鈣離子或鎂離子)，以提供含鎂氫氧基磷灰石穩定的成核。我們優化合成條件以獲得相對低結晶度的含鎂氫氧基磷灰石，透過 X 光繞射分析儀測量證明其晶相與人體骨骼相似。在體外試驗中，含鎂氫氧基磷灰石中的鎂離子釋放有利於骨細胞的增生和分化。綜上所述，這項研究闡述磷脂質應用於含鎂氫氧基磷灰石的新功效，並提供一種具前景的骨科生醫材料。

關鍵字：鎂、氫氧基磷灰石、磷脂質、骨修復材料、人類骨母細胞(MG63)。

Table of Content



Abstract	i
摘要	ii
Table of Content	iii
List of Figures	vi
List of Tables	viii
1. Introduction	1
1.1. Biomaterials for bone graft.....	1
1.2. Calcium phosphate	4
1.3. Magnesium loaded hydroxyapatite.....	9
1.4. Phospholipid	13
2. Objectives	17
3. Experimental.....	18
3.1. Chemicals and Materials	18
3.2. Equipment.....	20
3.3. Preparation of Mg@HAp and Mg@HAp-PC.	22
3.3.1. Synthesis of Mg@HAp	22
3.3.2. Synthesis of Mg@HAp-PC	24
3.4. Characterization.....	26
3.4.1. X-ray Diffractometer (XRD)	26
3.4.2. Field Emission Scanning Electron Microscope (FE-SEM).....	26
3.4.3. Inductively Coupled Plasma-Mass Spectrometer (ICP/MS)	27
3.4.4. High Resolution Transmission Electron Microscope (HRTEM)....	27
3.4.5. Fourier Transform Infrared Spectrometer (FTIR)	27

3.4.6.	X-ray Photoelectron Spectroscopy (XPS)	28
3.4.7.	Zeta Potential Analyzer	28
3.4.8.	Degradation test.....	28
3.4.9.	Cell Culture	29
3.4.10.	MTT Assay	29
3.4.11.	ALP Assay	32
3.4.12.	Quantitative analysis of Mg ions release.....	35
3.4.13.	Statistical analysis	35
4.	Results and Discussion	36
4.1.	Materials characterizations	36
4.2.	PC-assisted reaction mechanism	53
4.3.	Degradation test.....	56
4.4.	<i>In vitro</i> test.....	57
4.4.1.	Cell viability and proliferation	57
4.4.2.	Cellular differentiation	59
4.4.3.	Quantitative analysis of Mg ions release.....	60
5.	Conclusion.....	62
6.	Future Prospects.....	63
7.	Reference.....	64
Appendix	69	
A.1	ICP calibration curve of (a) magnesium, (b) calcium and (c) phosphorus ...	69
A.2	EDS of Mg@HAp and Mg@HAp-PC	71
A.3	The specific surface area of Mg@HAp and Mg@HAp-PC	71
A.4	Adsorption and desorption isotherms of (a) Mg@HAp and (b) Mg@HAp-PC	72

A.5	The mesoporous pore distribution of (a) Mg@HAp and (b) Mg@HAp-PC	73
A.6	The microporous pore distribution of (a) Mg@HAp and (b) Mg@HAp-PC	74
A.7	The XRD pattern of HAp (Ca/Mg=0.5)	75
A.8	TGA analysis of HAp-PC (Ca/Mg=5)	75
A.9	Hydrodynamic size of Mg@HAp and Mg@HAp-PC.....	76

List of Figures

Figure 1.1	The hierarchical structure of typical bone	3
Figure 1.2	XRD patterns of natural bone	8
Figure 1.3	A schematic of bioapatite	12
Figure 1.4	The structure of a phospholipid	13
Figure 1.5	The structure of phosphatidylcholine.....	16
Figure 3.1	Typical process for preparing Mg@HAp.....	23
Figure 3.2	Typical process for preparing Mg@HAp-PC	25
Figure 3.3	Concept of MTT assay	30
Figure 3.4	Concept of ALP assay	32
Figure 4.1	FTIR analysis of HAp and HAp-PC	37
Figure 4.2	The XRD pattern of HAp and HAp-PC.....	37
Figure 4.3	The XRD comparison of (a) the different aging time of the HAp (Ca/Mg=5), (b) HAp-PC (Ca/Mg=5) and (c) HAp-1.5PC (Ca/Mg=5) crystallization ..	40
Figure 4.4	The XRD pattern of HAp (Ca/Mg=5) and HAp-PC (Ca/Mg=5).....	42
Figure 4.5	The TEM image of (a)(b) HAp (Ca/Mg=5) and (c)(d) HAp-PC (Ca/Mg=5).....	43
Figure 4.6	The XRD pattern of (a) HAp (Ca/Mg=10), HAp (Ca/Mg=5) and HAp (Ca/Mg=1) (b) HAp-PC (Ca/Mg=10), HAp-PC (Ca/Mg=5) and HAp-PC (Ca/Mg=1).	46
Figure 4.7	SEM image of (a) HAp (b) HAp-PC (c) HAp (Ca/Mg=10) (d) HAp-PC (Ca/Mg=10) (e) HAp (Ca/Mg=5) (f) HAp-PC (Ca/Mg=5) (g)(i) HAp (Ca/Mg=1) (h)(j) HAp-PC (Ca/Mg=1).....	48
Figure 4.8	Zeta potential of Mg@HAp and Mg@HAp-PC	48
Figure 4.9	FTIR analysis of HAp and HAp-PC (Ca/Mg=5)	51
Figure 4.10	XPS analysis of HAp and HAp-PC (Ca/Mg=5)	52

Figure 4.11 Principle of the nucleation on the surface of liposome vesicles in the reaction synthesized.....	54
Figure 4.12 Process for preparing HAp-Ca occupied PC (Ca/Mg=5)	54
Figure 4.13 Degradation of Mg@HAp and Mg@HAp-PC for various time periods ..	56
Figure 4.14 Cytotoxicity of various concentrations of Mg@HAp and Mg@HAp-PC in 1 day of culture	58
Figure 4.15 Proliferation assay of HAp and Mg@HAp-PC	58
Figure 4.16 Differentiation assay of HAp and Mg@HAp-PC	59

List of Tables

Table 1.1	Calcium phosphates used in the biomaterial field	7
Table 1.2	The conditions of synthesis for Mg substituted HAp	12
Table 1.3	Different kinds of phospholipids with polar group R and net charge.....	14
Table 3.1	Chemicals and materials	18
Table 3.2	List of equipment.....	20
Table 3.3	The sample label and adjusted parameters for Mg@HAp	23
Table 3.4	The sample label and adjusted parameters for Mg@HAp-PC	25
Table 3.5	Measurement conditions of XRD	26
Table 4.1	ICP/MS of Mg@HAp and Mg@HAp-PC.....	51
Table 4.2	ICP/MS of Mg@HAp-PC in different process.....	55
Table 4.3	The Mg ions release and uptake of cell in 3 days	61

1. Introduction

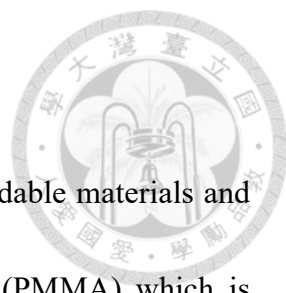


1.1. Biomaterials for bone graft

Bone possesses the intrinsic ability to regeneration as part of the repair process in response to injury, as well as during skeletal development or remodelling in adulthood. The majority of bone injuries heal which is eventually indistinguishable from the adjacent uninjured bone, and the bone restores its original properties. However, there are still cases of fracture in which bone regeneration is impaired, such as large bone defects observed after bone tumor resection and severe nonunion fractures.^{1, 2}

In cases where bone defects are not self-regeneration, methods involving autologous or allogeneic bone grafts and synthetic bone substitute materials should be used. However, problems such as cost, painfulness, hematoma and inflammation with donor-site morbidity in autologous. Similarly, allogeneic also have limitations for the risks of rejection by the patient's immune system and the possibility of infection or disease from the donor. The orthopedic biomaterials treatment market is growing rapidly due to urgent clinical needs. In 2017, the demand for orthopedics and implants is the fourth largest medical product in the world. Currently, materials for biomedical ceramic bone filling have been used to implant bone defects to accelerate bone tissue repair, of which properties including good bioabsorbable, osteoconductive, osteoinductive and

biocompatible development.^{3, 4}



Bone graft materials can be mainly divided into non-biodegradable materials and biodegradable materials. For example, poly(methyl methacrylate) (PMMA) which is known as bone cement, is non-biodegradable materials. On the other hand, biodegradable materials, for instance, bioceramic and polymer, are one of the most popular research topics for bone tissue engineering. Bioactive inorganic materials, e.g. tricalcium phosphate, hydroxyapatite (HAp), bioactive glasses and their combinations, have been attractive due to their biocompatibility. Although inorganic ceramics do not possess osteoinductive capacity, they certainly have bone conduction capacity and significant ability to directly bind to the bone. And the inorganic ceramic material is shadowed by the fact that it is poor for fracture toughness and unsuitable load-bearing applications. Biodegradable polymers include natural sources of chitin, collagen, and gelatin, or synthetic polycaprolactone (PCL), polyglycolic acid (PGA), polylactic acid (PLA), etc. Synthetic polymers can be produced under controlled conditions and therefore typically exhibit predictable and reproducible mechanical and physical properties such as tensile strength, modulus of elasticity and rate of degradation. However, some polymers have acidic degradation products, and could cause a strong inflammatory reaction when suddenly release. In addition to the main classifications mentioned above, composite materials are also rapidly developing and proved to be promising. To mimic the inorganic-

organic composite of natural bone, combination of a tough polymer with the compressive strength and inorganic materials with bioactive is applied which improves mechanical properties and degradation profiles. However, it remains challenging for mineral and organic components to recreate the same degree of nanoscale orientation as natural bone. The most significant organic component in the bone structure is collagen, which promotes the production of nanosize crystals of HAp aligned in the cortical bone (**Figure 1.1**). However, it remains a mystery that how the highly ordered structure is formed from the combination of the organic and inorganic molecules.⁵⁻⁷

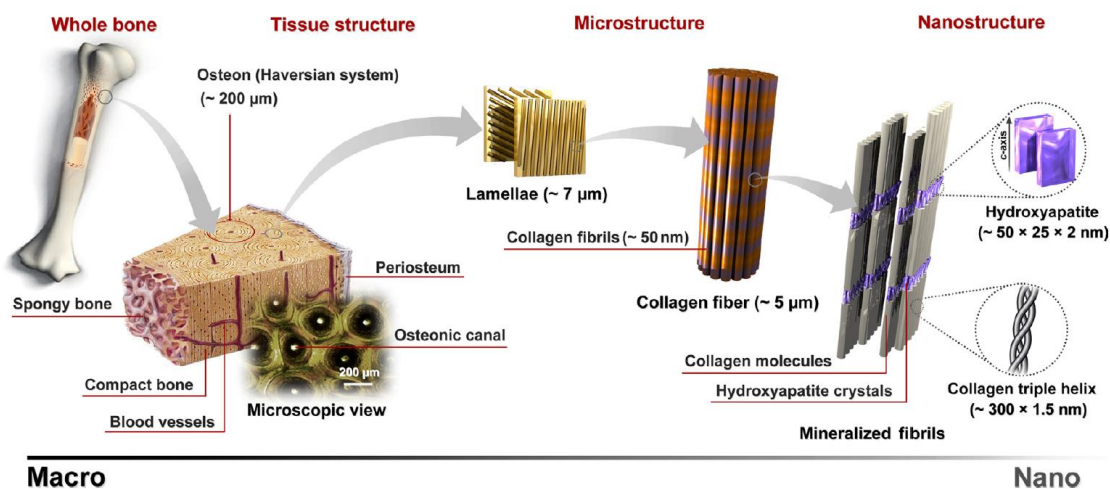
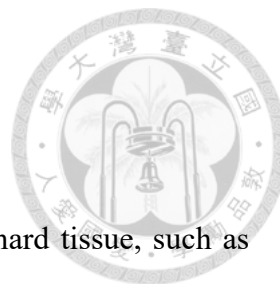


Figure 1.1 The hierarchical structure of typical bone⁸



1.2. Calcium phosphate

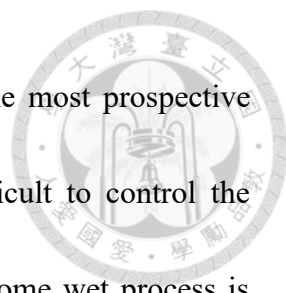
Calcium phosphate (CaP) composes the main part of bodily hard tissue, such as bone and teeth. CaP has been the most promising investigated among various inorganic materials for the biomedical field. CaP superior to other inorganic materials is owing to its properties which are similar in composition to bone mineral and their excellent biodegradability, bioactivity and osteoconductivity. Nevertheless, it is known that CaPs have relatively low mechanical properties; therefore, they cannot provide sufficient structural support and are unsuitable for application in load bearing areas. The types of various CaP are shown in **Table 1.1**. The synthesis method and process parameters for CaP have a significant effect on the stoichiometry of the synthesized product, its crystallinity, particle size, bioceramic phase composition, thermal stability, microstructure and mechanical properties. And the important process parameters affecting the properties of CaP synthesis products are temperature, pH value, reagent type, concentration, purity and quality.^{9, 10}

For bone graft, currently, the most commonly used CaP in clinically tested are HAp, β -tricalcium phosphate (β -TCP) and biphasic HAp/ β -TCP mixture. It could be made into a form of the block, granule, sheet, or even molded into the desired shape for using in surgery. HAp has long degradation times *in vivo*, usually in for months or even years. The

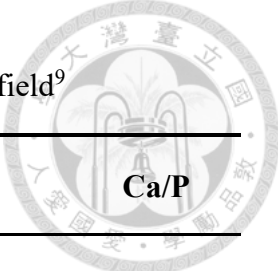
rate of dissolution of the synthetic HAp depends on the concentration and the pH of the solution, the solid/solution ratio, and the composition and crystallinity of the HAp phase.

In the case of crystalline HAp, the distribution of micropores and macropores, the defects and the type of other phases present also have a significant degradation effect. The dissolution rate of CaP is in the following order: amorphous HAp > β -TCP > crystalline HAp.⁷ As a result of the similarity of the crystalline phase between low crystallinity HAp and the mineralized of natural bone matrix (**Figure 1.2¹¹**), HAp has been the most generally researched apatite in bone tissue engineering. In addition, it is thermodynamically the most stable crystalline phase of CaP. That is the reason why it stands out among numerous calcium phosphate materials. HAp is commonly applied in material for biomedical, such as a replacement for bony and periodontal defects, middle ear implants, bone tissue engineering, drug delivery agent, dental materials and coating on metallic implants.⁸ Although the applications of HAp are limited due to some disadvantages such as the limited stimulation of the new bone tissue growth and insignificant degradation in the recovery period, its bioactivity and biodegradation can be modified through substitutions of other anions, cations, or functional groups.^{12, 13}

The preparation method of HAp can be divided into wet, dry, high-temperature, synthesis from biogenic sources, and combination procedures method. Each preparation method has its advantages and disadvantages. For the most universal wet method, it can



accurately control the morphology and size of particles, and be the most prospective methods for the synthesis of nanosized HAp. However, it is difficult to control the crystallinity and phase purity of particles in aqueous solution, so some wet process is unsuitable for scaling up of HAp quantities. Dry methods including solid-state synthesis and the mechanochemical process, their conditions do not require precisely controlled, owing to the characteristics of powder that are not highly affected by the processing parameters. Therefore, this method is suitable for mass production. However, the disadvantage of using the solid-state synthesis and the mechanochemical process are the big size of particles and the low purity of HAp, respectively. High-temperature processes are often used to synthesize high crystallinity and purity phase of HAp, but it is poorly controlled the processing variables. Additionally, the high crystallinity of HAp from this synthesized method is opposite to bioapatite characteristics. The synthesis from biogenic sources is to extract the biominerals from biowastes, such as bovine bones, eggshells and the exoskeleton of marine organisms. Although its physicochemical similarity to the human bone and have the economic and environmental benefits of waste recovery, the modification for HAp is not be achieved conveniently during the synthesis process.⁸ Considering the advantages and disadvantages of the above, the wet synthesis is still a more suitable method.

Table 1.1 Calcium phosphates used in the biomaterial field⁹


Name	Abbreviation	Chemical formula	Ca/P
Amorphous calcium phosphate	ACP	$\text{Ca}_x\text{H}_y(\text{PO}_4)_z \cdot n\text{H}_2\text{O}$	1.2-2.2
Dicalcium phosphate anhydride	DCPA	CaHPO_4	1.00
Dicalcium phosphate dehydrate	DCPD	$\text{CaHPO}_4 \cdot 2\text{H}_2\text{O}$	1.00
Octacalcium phosphate	OCP	$\text{Ca}_8(\text{HPO}_4)_2(\text{PO}_4)_4 \cdot 5\text{H}_2\text{O}$	1.33
β -tricalcium phosphate	β -TCP	$\text{Ca}_3(\text{PO}_4)_2$	1.50
α -tricalcium phosphate	α -TCP	$\text{Ca}_3(\text{PO}_4)_2$	1.50
Hydroxyapatite with calcium deficient	CDHA	$\text{Ca}_{10-x}(\text{HPO}_4)_x(\text{PO}_4)_{6-x}(\text{OH})_{2-x}$ $0 \leq x \leq 1$	1.5-1.67
Hydroxyapatite	HAp	$\text{Ca}_{10}(\text{PO}_4)_6(\text{OH})_2$	1.67
Tetra calcium phosphate	TTCP (TetCP)	$\text{Ca}_4(\text{PO}_4)_2\text{O}$	2.00
β -Ca pyrophosphate	CPP	$\text{Ca}_2\text{P}_2\text{O}_7$	<1.5
Oxyapatite	OAp	$\text{Ca}_{10}(\text{PO}_4)_6\text{O}$	1.67

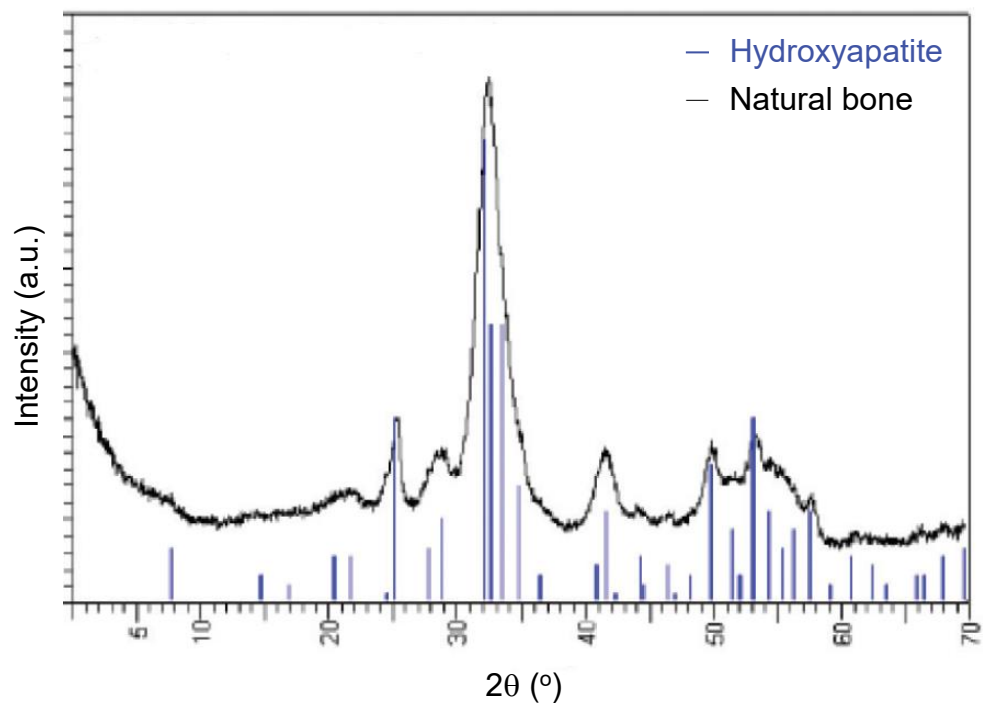


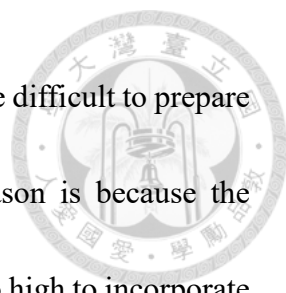
Figure 1.2 XRD patterns of natural bone¹¹



1.3. Magnesium loaded hydroxyapatite

Mg possesses a mechanical property closed to natural bone, and higher stiffness than ceramic biomaterials. It is proved that Mg or Mg alloys are a potential and biodegradable orthopedic implant for the reconstruction of bone defects *in vivo* experiments and even indicated that Mg is osteoinductive and promotes the remodelling of bone. Besides, Mg ions can increase the adhesion, growth and alkaline phosphatase (ALP) activity of osteoblasts and bone mesenchymal stem cells (BMSCs), resulting in promoting the differentiation and enhancing bone formation and integration with host bone.¹⁴ Although the induced inflammatory response of Mg or Mg alloys is relatively mild, it is quickly degraded *in vivo* and cannot provide continued mechanical support for fracture healing.^{15, 16}

The inorganic component of the biological bone is nonstoichiometric apatite which is low crystalline and contains cationic and anionic substitutions in the sites of the HAp crystal structure. Considering cationic substitutes, Mg ion is the most abundant and essential element that is crucial for bone health^{17, 18}. Approximately 50-60% of Mg is stored in the bone matrix of human body, acting as surface substituents of the HAp mineral component of bone. A schematic of bioapatite is shown in **Figure 1.3**¹⁹. However, Mg plays an inhibitor in the crystallization process of calcium phosphate and destabilizes



the structure of HAp. Additionally, pure high Mg-content minerals are difficult to prepare in aqueous solution and at physiological temperature²⁰⁻²². The reason is because the hydration energy of the magnesium in the aqueous environment is too high to incorporate the Mg in the mineral crystal structure²³. The maximum of Mg incorporation in synthetic HAp is about 0.4 wt%. However, there are still methods to increase the content of magnesium in HAp. Such as adding other ions (e.g. carbonate or fluoride) as paired substitutions simultaneously incorporated with Mg. There are some effects for HAp properties by increasing the content of Mg in HAp: (i) the crystallinity decreasing, (ii) the incorporation of HPO_4^{2-} increasing, and (iii) the extent of dissolution increasing.^{24, 25}

Mg containing HAp is widely studied; however, the Mg content of pure HAp is still limited. Ren *et al.*²⁶ synthesized the substitution of Mg in HAp by the wet-chemical precipitation method at 90 °C and the upper limit of Mg substitution ($\text{Mg}/(\text{Mg} + \text{Ca})$) in HAp between 5 and 7 mol%. Liangzhi *et al.*¹⁴ managed to synthesize Mg-substituted HAp whiskers by hydrothermal method with acetamide as a homogeneous precipitation reagent. The molar ratio of $\text{Mg}/(\text{Mg} + \text{Ca})$ could be facilely changed from 1.61 to 6.14 mol%. Cacciotti *et al.*²⁷ reported Mg substituted HAp nanopowders whose Mg content ranged between 0.6 and 2.4 wt%. Landi *et al.*¹⁷ used wet-chemical synthesis to synthesize HAp doped with different Mg amount. The ion doping of the Mg-substituted HAp is up to 3.2 wt%. With the mechanochemical-hydrothermal technique at room temperature,

Suchanek *et al.*²⁴ prepared Mg-substituted crystalline HA containing 0.24 to 28.2 wt% of Mg; however, the highest Mg-substituted amount of material is impure HAp which $\text{NH}_4\text{MgPO}_4 \cdot \text{H}_2\text{O}$ were detected. The above mentioned experimental conditions are shown in **Table 1.2**. Until now, the research and applications of the Mg-containing biomaterials is still a popular research theme.

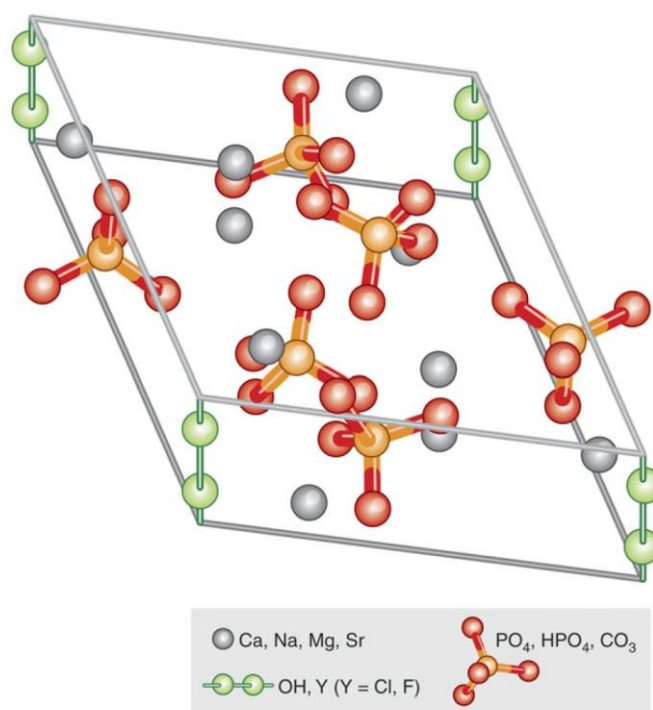


Figure 1.3 A schematic of bioapatite¹⁹

Table 1.2 The conditions of synthesis for Mg substituted HAp

Mg/(Mg+Ca) (%)	Mg (wt%)	Reaction temp. (°C)	Reaction time (hr)	Dry temp. (°C)	Dry time (hr)	Reference
5-7	-	90	5	100	10	26
1.61-6.14	-	180	10	200	48	14
-	0.6-2.4	room	24	60	-	27
-	0.7-3.2	25	24	Freeze	-	17
-	0.24-28.2	25-33	5	70	24	24



1.4. Phospholipid

Lipid has good biocompatibility due to it is the major compositions in biological membranes. Lipid is amphiphilic molecule and the most abundant class of lipid in cell membranes is phospholipids.²⁸ The phospholipid molecules consist of a polar head, a phosphate group, and two non-polar fatty acid chain tails one of which is usually one unsaturated. The hydrophilic head group is polar, zwitterionic or charged. The structure of a phospholipid is shown in **Figure 1.4**, and the R group of the polar head attached to the phosphate typically determines the lipid type²⁹, including phosphatidic acid (PA), phosphatidylethanolamine (PE), phosphatidylcholine (PC), phosphatidylserine (PS), phosphatidylglycerol (PG), phosphatidylinositol 4,5-bisphosphate (PIP2), cardiolipin (CL) (**Table 1.3**).

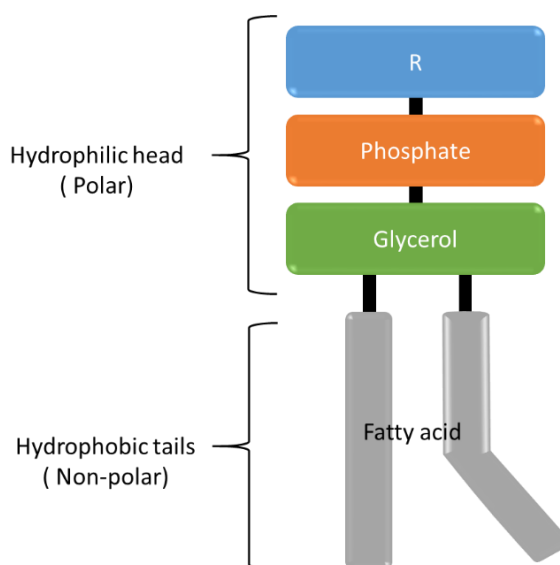
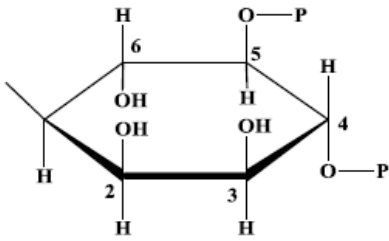
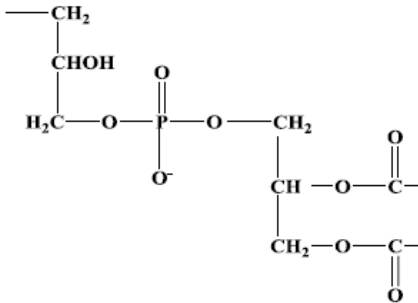
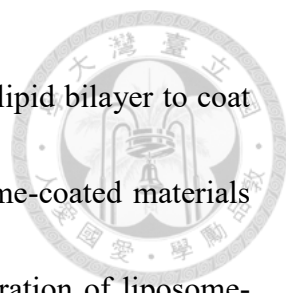


Figure 1.4 The structure of a phospholipid²⁹

Table 1.3 Different kinds of phospholipids with polar group R and net charge²⁹

Phospholipid	R	Formula of R	Net Charge at pH 7
PA	-	—H	-1
PE	Ethanolamine	—H ₂ C—CH ₂ —NH ₃ [⊕]	0
PC	Choline	—H ₂ C—CH ₂ —N [⊕] (CH ₃) ₃	0
PS	Serine	$\begin{array}{c} \text{—H}_2\text{C—CH—NH}_3^{\oplus} \\ \\ \text{COO}^- \end{array}$	-1
PG	Glycerol	$\begin{array}{c} \text{—CH}_2\text{—CH—C—OH} \\ \quad \quad \\ \text{OH} \quad \text{H}_2\text{O} \end{array}$	-1
PIP2	Inositol 4,5-bisphosphate		-4
CL	Phosphatidylglycerol		-2



Huang *et al.*³⁰ used liposomes which are vesicles formed of a lipid bilayer to coat on HAp and TCP as bone implants. They observed that the liposome-coated materials were biocompatible and their clinical results were enhanced. Preparation of liposome-coated HAp with controlled morphology and size distribution; therefore, may be beneficial to therapy of bone disease and applications. Additionally, Feng *et al.*³¹ and Chu *et al.*³² have used liposomes to synthesize HAp and calcium phosphate, they purposed to discuss the role of the vesicle membrane in the controlled precipitation of calcium phosphate. The calcium phosphate synthesized in the presence or absence of liposomes were both low crystalline, and had a chemical composition similar to natural HAp.

Although the synthesis of HAp by using liposome as a model has been investigated, there is no study on the substitution of Mg ions in the lattice of HAp in a lipid system. Lipids are classified into zwitterionic like phosphatidylcholine (**Figure 1.5**), which would have the negatively charged lipid phosphate functional group to interact with Ca and Mg ions.³³⁻³⁵ Yu *et al.*³⁶ prepared mesocrystals of high-magnesian calcite in lipid solution. Therefore, it is conceivable that the external surface of the liposome vesicles is involved in the nucleation of Mg-loaded HAp (Mg@HAp) particles.

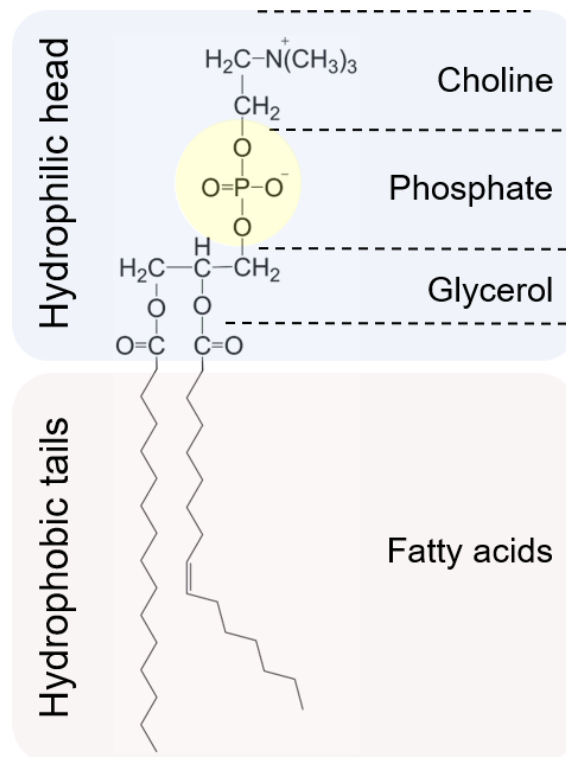


Figure 1.5 The structure of phosphatidylcholine

2. Objectives



Production of Mg-substituted HAp has been investigated by a lot of researchers in recent years. However, all of them introduce limited content of Mg in HAp or impure crystalline phase of HAp. We propose is that the negatively charged lipid phosphate functional group could act on cations that provided a stable nucleation space for Mg@HAp. In this study, we combine the bioactive Mg@HAp and the PC as an inorganic-organic composite material. Through the PC-assisted synthesis, we synthesize a higher amount of Mg in HAp compared with the process involving no PC. Furthermore, we will propose a possible mechanism for the PC-assisted synthesis procedure. In this work, we aim to synthesize pure Mg@HAp powders with controllable Mg contents which possess bioactivity, biocompatibility, osteoconductivity, and bioresorbability for bone healing material.


3. Experimental



3.1. Chemicals and Materials

Table 3.1 Chemicals and materials

Chemical	Formula	Manufacturer
Calcium chloride	CaCl_2	Sigma-Aldrich
Magnesium chloride	MgCl_2	Sigma-Aldrich
Diammonium hydrogenphosphate	$(\text{NH}_4)_2\text{HPO}_4$	Sigma-Aldrich
L- α -Phosphatidylcholine (PC)	-	Sigma-Aldrich
Ethyl Acetate (EA)	$\text{CH}_3\text{COOC}_2\text{H}_5$	Honeywell
Sodium hydroxide	NaOH	Sigma-Aldrich
Hydrochloric acid	HCl	Honeywell
Nitric acid	HNO_3	Honeywell
Potassium bromide	KBr	Sigma-Aldrich
Dulbecco's Phosphate Buffered Saline (DPBS)(10X)	-	Biological Industry
Minimum Essential Medium alpha (MEM- α)	-	Gibco



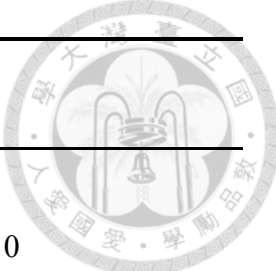
Chemical	Formula	Manufacturer
Fetal bovine serum (FBS)	-	Gibco
Pen-Strep-Ampho.B	-	Biological Industry
Dimethyl sulfoxide	$(\text{CH}_3)_2\text{SO}$	Sigma-Aldrich
Trypsin-EDTA (10X)	-	Biological Industry
Thiazolyl Blue Tetrazolium Bromide	$\text{C}_{18}\text{H}_{16}\text{BrN}_5\text{S}$	Sigma-Aldrich
Triton™ X-100	-	Sigma-Aldrich
2-Amino-2-methyl-1-propanol	$(\text{CH}_3)_2\text{C}(\text{NH}_2)\text{CH}_2\text{OH}$	Sigma-Aldrich
4-Nitrophenyl phosphate disodium salt hexahydrate (pNPP)	$\text{O}_2\text{NC}_6\text{H}_4\text{OP}(\text{O})(\text{ONa})_2 \cdot 6\text{H}_2\text{O}$	Sigma-Aldrich
Tris-HCl Buffer	-	Sigma-Aldrich
Magnesium chloride hexahydrate	$\text{MgCl}_2 \cdot 6\text{H}_2\text{O}$	J.T.Baker
4-Nitrophenol (p-NP)	$\text{O}_2\text{NC}_6\text{H}_4\text{OH}$	Sigma-Aldrich
Trypan blue stain	-	Gibco

3.2. Equipment

Table 3.2 List of equipment



Equipment	Manufacturer
pH meter	HACH SensION+ PH31
Rotary evaporator	KNF RC600
Sonicator	DELTA
Water bath	HOTECH
Shaker	LMS VTX-3000L
Centrifugator	SIGMA 3-30KS
Lyophilizer	EYELA FDU-1200
X-ray diffractometer (XRD)	Rigaku
Fourier-Transform Infrared Spectrometer (FTIR)	Perkin Elmer Spectrum 100
Zeta Potential Analyzer	Malvern, Zetasizer Nano
Field Emission Scanning Electron Microscope (FE-SEM)	Hitachi S-4800
Inductively Coupled Plasma-Mass Spectrometer (ICP/MS)	Agilent



Equipment	Manufacturer
High-resolution transmission electron microscopy (HRTEM)	JEOL JEM-2010
Centrifugator	KUBOTA 2420
Optical microscopy	LEICA DMI3000 B
Incubator	ESCO
ELISA Reader	TECAN Sunrise



3.3. Preparation of Mg@HAp and Mg@HAp-PC.

3.3.1. Synthesis of Mg@HAp

$(\text{NH}_4)_2\text{HPO}_4$ (0.12 M) was dissolved in DI water (125 mL). CaCl_2 (x M) and MgCl_2 (y M) were added together into DI water (125 mL) in a vial. The total cation ion concentration is 0.12 M ($x + y = 0.12$). The sample label and the parameters of Ca/Mg concentration being adjusted were shown in **Table 3.3**. To dissolve the solid, both of the solutions were stirred for 10 minutes. The pH value of the two solutions were respectively adjusted to 9.00 by NaOH. Then, Ca/Mg solution was dropwise added into $(\text{NH}_4)_2\text{HPO}_4$ solution for 2 mL/min, and stirred for 15 minutes. The solution was incubated under quiescence and physiological temperature at 37 °C for 19 hours in water bath. After aging 19 hours, the solution was centrifuged at 20000 $\times g$ for 5 minutes. The resulting solid was washed by DI water for 5 times. The result product was dried by the lyophilizer for at least 24 hours. Typical process is shown in **Figure 3.1**.

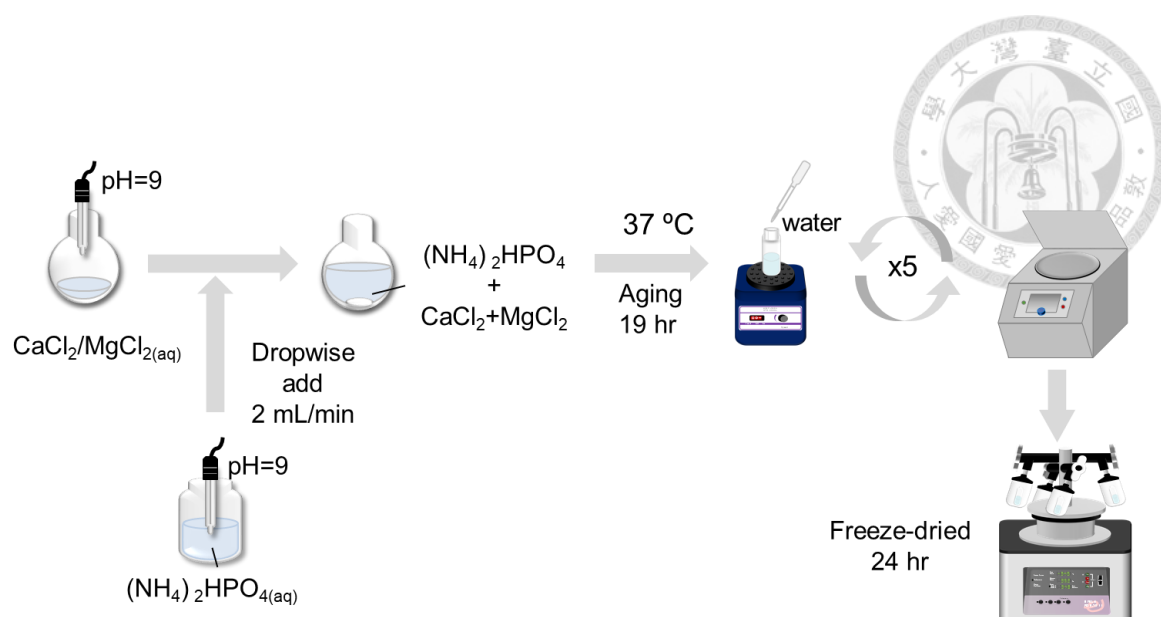


Figure 3.1 Typical process for preparing Mg@HAp

Table 3.3 The sample label and adjusted parameters for Mg@HAp

Sample	Concentration of Ca^{2+} (M)	Concentration of Mg^{2+} (M)
HAp	0.12	0
HAp (Ca/Mg=10)	0.109	0.0109
HAp (Ca/Mg=5)	0.1	0.02
HAp (Ca/Mg=1)	0.06	0.06



3.3.2. Synthesis of Mg@HAp-PC

A lipid thin film was prepared by dissolving 4.5 mmol of L- α -phosphatidylcholine (PC) from soybean in 30 mL of ethyl acetate (EA) with sonication for 15 minutes, followed by rotary evaporation at 100 rpm, 40 °C for 10 minutes. The solution of 125 mL of CaCl₂ (x M) and MgCl₂ (y M) at pH 9.00 was mixed with the PC film. The total cation ion concentration is 0.12 M ($x + y = 0.12$). The sample label and the adjusted parameters of Ca/Mg concentration and PC were shown in **Table 3.4**. After the solution mixture was sonicated for 20 minutes and adjusted to pH 9.00, the 125 mL of (NH₄)₂HPO₄ solution (0.12 M, pH 9.00) was dropwise added into it with 2 mL/min and stirred for 15 minutes. The solution was incubated under quiescence and physiological temperature at 37 °C for 19 hours in water bath. After aging 19 hours, the final pH value was in the range of 7.0 to 7.6. After an addition of 10 mL of EA to the solution mixture, the precipitate of calcium phosphate was collected by centrifugation (20000 \times g for 5 minutes) and the unreacted PC was removed by EA. Additional of 10 mL DI water and 10 mL EA was added to wash the solid for 5 times. The solid sample was finally dried with the lyophilizer for at least 24 hours. Typical process is shown in **Figure 3.2**.

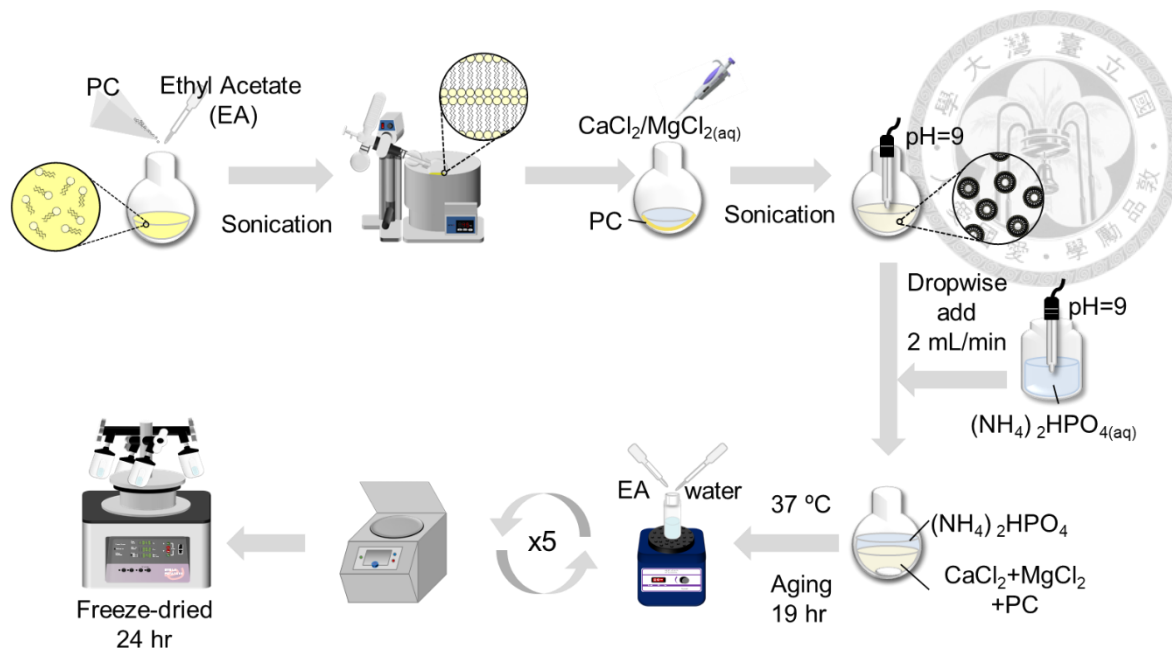


Figure 3.2 Typical process for preparing Mg@HAp-PC

Table 3.4 The sample label and adjusted parameters for Mg@HAp-PC

Sample	Concentration of Ca^{2+} (M)	Concentration of Mg^{2+} (M)	Amount of phosphatidylcholine (mmol)
HAp-PC	0.12	0	4.5
HAp-PC (Ca/Mg=10)	0.109	0.0109	4.5
HAp-PC (Ca/Mg=5)	0.1	0.02	4.5
HAp-PC (Ca/Mg=1)	0.06	0.06	4.5
HAp-1.5PC (Ca/Mg=5)	0.1	0.02	6.75



3.4. Characterization

3.4.1. X-ray Diffractometer (XRD)

Wide-angle patterns of powder X-ray diffraction pattern (XRD) were measured on Rigaku Ultima IV with Cu K α radiation ($\lambda=1.5418$ Å) to identify the crystal structure of calcium phosphate. All measurement conditions were listed in **Table 3.5**.

Table 3.5 Measurement conditions of XRD

Condition	Value
X-ray source	Cu K α
Wavelength (λ)	1.5418 Å
Voltage	40
Current	40
Angle range (2 theta)	10-60
Scan speed	10 °/min

3.4.2. Field Emission Scanning Electron Microscope (FE-SEM)

The morphology of the samples was observed by FE-SEM (Hitachi S-4800). All the samples were taped on the carbon conductive tape. Before SEM observation, the samples were kept under vacuum to remove the moisture content, and were sputtered by Pt coating in 10 kV operating voltage.

3.4.3. Inductively Coupled Plasma-Mass Spectrometer (ICP/MS)

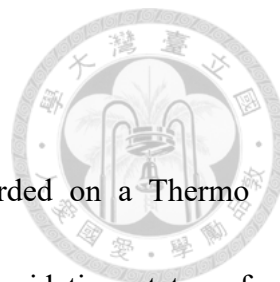
Every sample (1 mg) was digested in 2 mL aqua regia ($\text{HNO}_3 : \text{HCl} = 1 : 3$ in v/v) and further diluted to 1000 ppb by 2 wt% nitric acid. All of the samples were purified by 0.2 μm filter to avoid the injection of any solid into the instrument. The calibration curves were built by magnesium, calcium and phosphorus standard solution of 0, 62.5, 125, 250, 500 and 1000 ppb, respectively. The calibration curves were shown in A.1.

3.4.4. High Resolution Transmission Electron Microscope (HRTEM)

To prepare the sample for analysis, 0.1 mg of each powder sample was dissolved in 5 mL ethanol and then sonicated for 30 minutes. The aqueous dispersions were drop-coated and dried onto copper grids. Finally, the copper grids were freeze dried with the lyophilizer for at least 24 hours.

3.4.5. Fourier Transform Infrared Spectrometer (FTIR)

Fourier transform infrared (FTIR) spectra were measured with Perkin Elmer Spectrum 100 at a resolution of 4 cm^{-1} . The spectrum was collected over the range of 4000-450 cm^{-1} . Samples for FTIR measurement were prepared by mixing vacuum-dried particles with potassium bromide (KBr) in appropriate ratio ($\text{KBr/sample} < 1:100$, w/w) and pressing into translucent discs.



3.4.6. X-ray Photoelectron Spectroscopy (XPS)

X-ray photoelectron spectroscopy (XPS) spectra were recorded on a Thermo Scientific K α X-ray photoelectron spectrometer to identify the oxidation states of magnesium and oxygen. Before measurement, the spectra were calibrated with reference to C1s at a binding energy of 284.5 eV.

3.4.7. Zeta Potential Analyzer

Zeta potential of samples were measured with Zetasizer Nano at 25 °C. Samples were sonicated for 1 hour with DI water as the solvent before the measurement. Each sample was done for three repeated.

3.4.8. Degradation test

Samples ($W_i = 50$ mg) mixed with PBS (10 mL) at 37 °C in thermostatic water bath for 1, 2, 3 and 4 weeks respectively. At predetermined time, the samples were centrifuged at 4000 $\times g$ for 10 minutes. Adding another 10 mL DI water for washing and centrifuging. The product was finally drying with the lyophilizer for at least 24 hours. The dry samples were weighed (W_f) to calculated the degradation rate using following equation:

$$\text{Degradation (\%)} = \frac{W_i - W_f}{W_i} \times 100$$

Degradation rate was recorded as mean \pm standard deviation for n=3.



3.4.9. Cell Culture

Human osteoblast-like cells (MG63) is used to evaluate the biocompatibility and proliferation of Mg-HAp particles in this study. MG63 were cultured in T75 containing 10 mL Minimum Essential Medium α (MEM- α). MEM- α contained 10 % Fetal bovine serum (FBS) and 1 % Pen-Strep-Ampho.B (P/S/A). The T75 were placed in the incubator for cell culture at 37 °C and 5 % CO₂ in air, and subcultured every 3 to 5 days.

3.4.10. MTT Assay

This study used the MTT assay as a test for cell viability and proliferation. The mitochondria are the most sensitive organelles in the cell to environmental factors, so their physiological status can represent the physiological state of the whole cell. MTT assay is the use of mitochondrial succinate dehydrogenases of living cells to convert the yellow water soluble MTT (3-(4,5-dimethylthiazol-2-yl)-2,5-diphenyltetrazolium bromide) dye into a purple insoluble formazan. The concept of MTT assay was shown in **Figure 3.3**. After the formazan was dissolved in DMSO, the absorbance can be used to determine the activity of the mitochondria, that is, the viability of cells. So, this method can be used to evaluate the compatibility of biomaterials for cell lines.

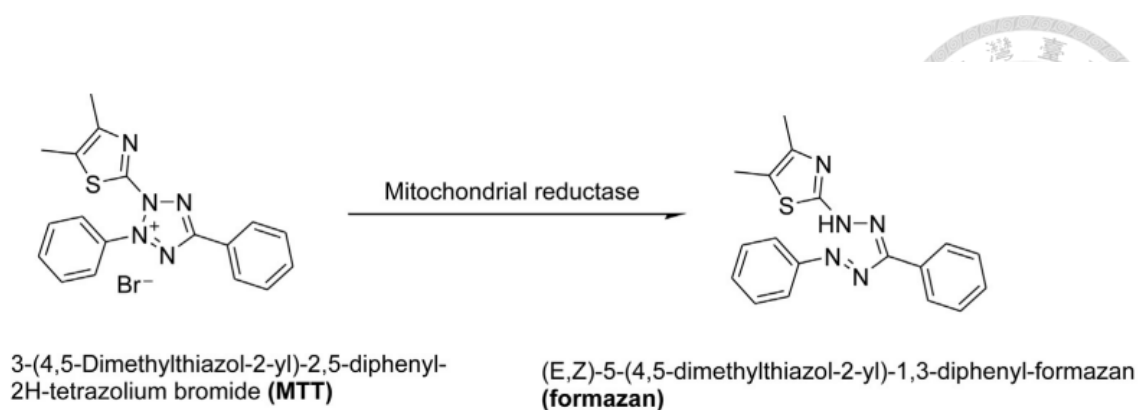


Figure 3.3 Concept of MTT assay³⁷

The standard procedures of MTT assay were as followed:

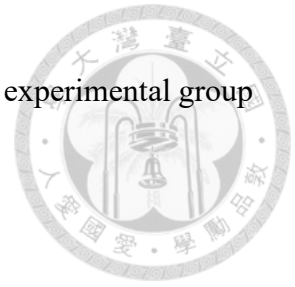
A. Preparation of chemicals

1. The MTT powder was dissolved in PBS at 5 mg/mL to prepare a stock solution, and sterilized by filtration using 0.2 μ m filter.
2. To store in a dark state, so wrapped the tube with aluminum foil and placed it in 4 °C refrigerator.
3. Diluted the stock solution at 0.5 mg/mL before used.

B. Procedures

1. 100 μ L of MG63 cell suspension (1×10^5 cells/mL) was transferred into each well of a 96-well cell culture plate. The cells were incubated at 37 °C for 24 hours in a humidified atmosphere containing 5 % CO₂.
2. Culture medium was replaced with 100 μ L of materials for the concentration: 0

mg/mL (control group), 0.1 mg/mL, 1 mg/mL, 10 mg/mL. Each experimental group was done for three repeated (n=3).



3. Incubated cells for 1, 3, 5, 7 and 14 days, separately.
4. The culture medium was aspirated from the plates, and washed by PBS twice. 100 μ L of the MTT solution was added to each well and the plate was further incubated for 3 hours at 37 °C.
5. MTT solution was replaced with 100 μ L of DMSO. The plate was incubated at room temperature for 10 minutes and subsequently subjected to a ELISA reader equipped with a 570 nm filter for colorimetric measurement.

3.4.11. ALP Assay

Alkaline phosphatase (ALP) is an enzyme of osteoblasts, and its expression activity is a distinct feature of osteoblast differentiation. ALP is considered to be an important indicator for the mineralization of bone and is a phenotypic marker for osteoblasts. Under alkaline conditions, ALP releases phosphate groups to react with 4-nitrophenyl phosphate (p-NPP). 2-Amino-2-methyl-1-propanol (AMP) is involved in the transfer of acyl phosphate, promoting the rate of enzyme reaction, and resulting in the formation of yellow p-nitrophenol (p-NP) from p-NPP. The concept of ALP assay was shown in **Figure 3.4**. ALP assay often used as an indicator of bone disease and clinical diagnosis. When the activity is increased, bone cancer and bone softening diseases such as rickets, fracture healing, osteoporosis, and bone malignant tumors can be found.

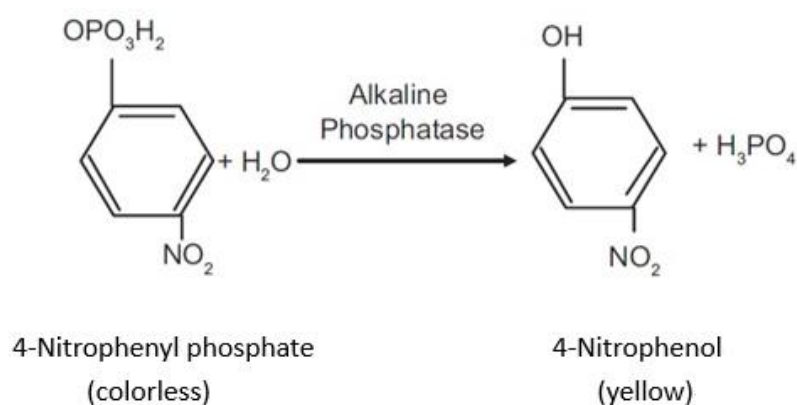


Figure 3.4 Concept of ALP assay³⁸



The standard procedures of ALP assay were as followed:

A. Preparation of chemicals

1. Prepared the p-NP solution for the concentration: 0, 6.25 μM , 12.5 μM , 25 μM , 50 μM and 100 μM .

2. 0.1 % Triton X-100


Chemical	Content
1 % Triton X-100	1 mL
0.1 M Tris buffer	9 mL

3. Substrate buffer

Chemical	Content
4-Nitrophenyl phosphate hexahydrate (p-NPP)	0.1856 g
2-Amino-2-methyl-1-propanol (AMP)	0.4845 g
Magnesium chloride hexahydrate	0.0407 g
DI water	100 mL

B. Procedures

1. 100 μL of MG63 cell suspension (1×10^5 cells/mL) was transferred into each well of a 96-well cell culture plate. The cells were incubated at 37 °C for 24 hours in a humidified atmosphere containing 5 % CO_2 .

- 
2. Culture medium was replaced with 100 μL of materials for the concentration: 0 mg/mL (control group) and 1 mg/mL. Each experimental group was done for three repeated ($n=3$).
 3. Incubated cells for 3, 5, 7 and 14 days, separately.
 4. The culture medium was aspirated from the plates, and washed by PBS twice.
 5. To release the ALP in the cell, 100 μL of the 0.1 % Triton X-100 solution was added to each well and the plate was further incubated for 1 hours at 37 $^{\circ}\text{C}$.
 6. In dark environment, took 50 μL of cell extract and p-NP solution (0, 6.25, 12.5, 25, 50, 100 μM) to 96-well plate and added 200 μL substrate buffer to each well for 1-hour incubation at 37 $^{\circ}\text{C}$.
 7. The reaction was terminated by adding 100 μL of 1 N NaOH.
 8. Used ELISA reader at 405 nm to acquire the absorbance.
 9. The calibration curves were built by the absorbance of p-NP standard solution of 0, 6.25, 12.5, 25, 50 and 100 μM respectively. The ALP content of sample were attained by substituting the absorbance into the calibration line.



3.4.12. Quantitative analysis of Mg ions release

MG63 were cultured in 96-well plate containing 100 μ L MEM- α with sample in 1 mg/mL. Incubated cells for 3 days, and aspirated the upper medium to measure the Mg concentration by ICP. It was calculated the Mg ions of cell uptake by using the blank test and original solution concentration.

3.4.13. Statistical analysis

Data represent the mean \pm standard deviation for three replicates. Statistical analysis was carried out on cellular tests using one-way analysis of variance (ANOVA). * represent the statistically significantly difference between sample and control (* $p < 0.05$, ** $p < 0.01$, *** $p < 0.001$).

4. Results and Discussion



4.1. Materials characterizations

The obtained materials are characterized to determine the PC effect on the HAp formation process in the Mg absence environment. In **Figure 4.1** and **Figure 4.2**, FTIR and XRD of aged 19h HAp and HAp-PC were shown. **Figure 4.1** shows the phosphate group of IR peak 602 and 561 cm^{-1} is assigned to ν_4 vibration of the PO_4^{3-} antisymmetric bending (O-P-O mode), which is the typical spectra of HAp phase^{39, 40}. The peak at 962 cm^{-1} is attributed to ν_1 (symmetric stretching mode) of PO_4^{3-} , and the peaks at 1027 and 1105 cm^{-1} to ν_3 (asymmetric stretching vibrational mode)⁴¹⁻⁴³. The peaks at 1640 and 1650 cm^{-1} are resulted from the vibrational of CO_3^{2-} ^{43, 44}. Opposite to the IR spectrum of HAp, the ester carbonyl band at 1740 cm^{-1} and the $\delta(\text{CH}_2)$ scissoring vibrations at 1466 cm^{-1} are observed in HAp-PC. Also, the signals observed between 2800 and 3100 cm^{-1} corresponding to the symmetric and asymmetric stretching vibrations from the CH_2 and CH_3 groups^{29, 45}. In the XRD comparison of **Figure 4.2**, the HAp synthesized in the PC system has lower crystallinity than the control experiment without PC. The dark inverted triangle indicates the position of the characteristic peaks of HAp.

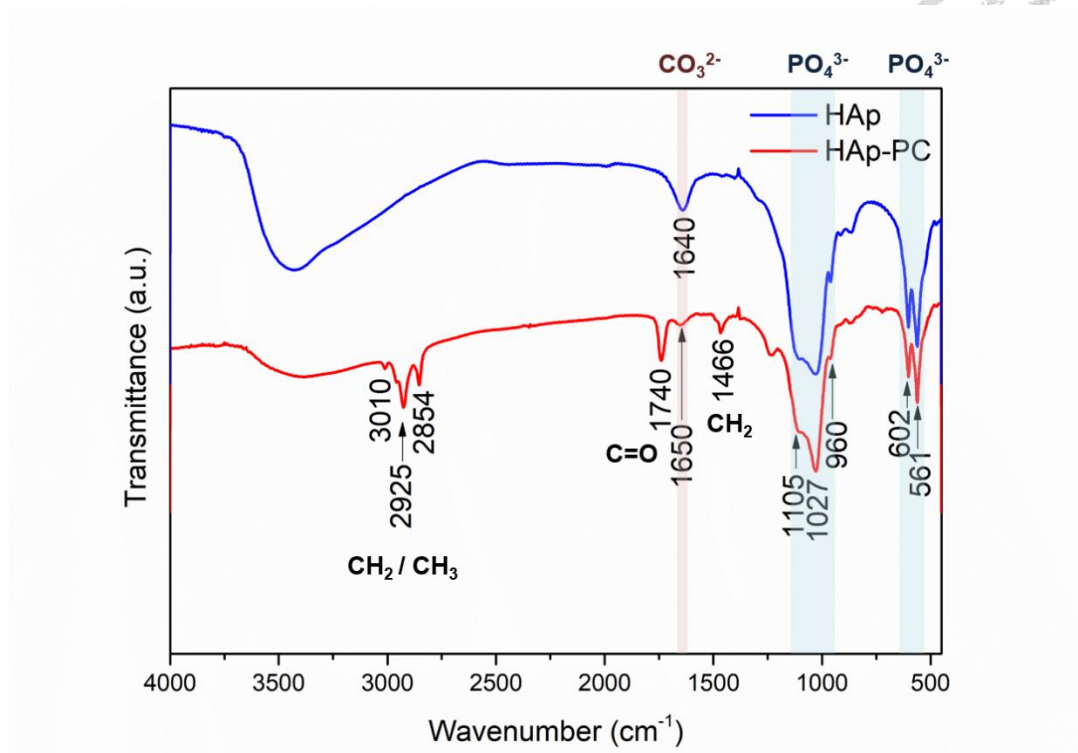


Figure 4.1 FTIR analysis of HAp and HAp-PC

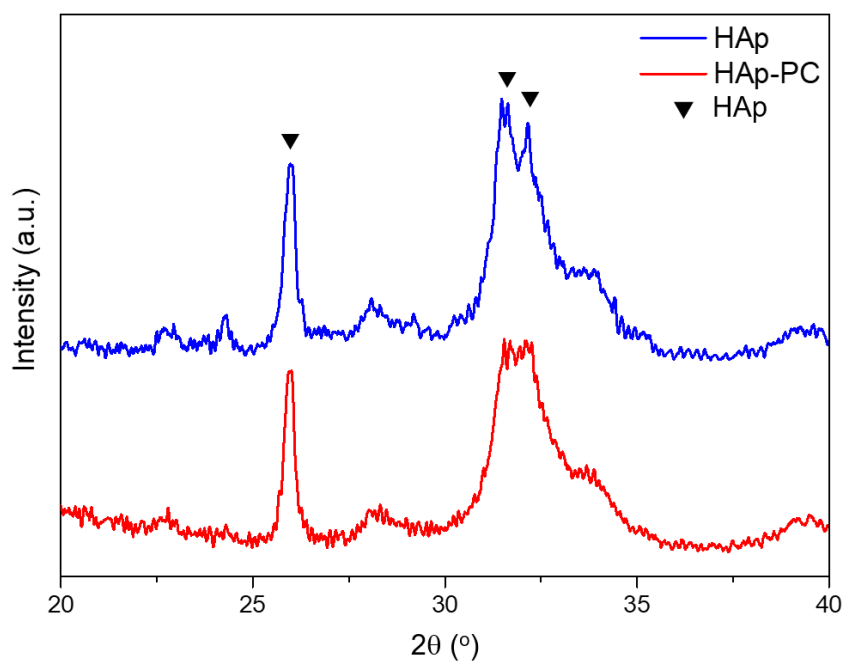
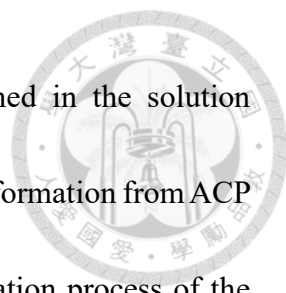
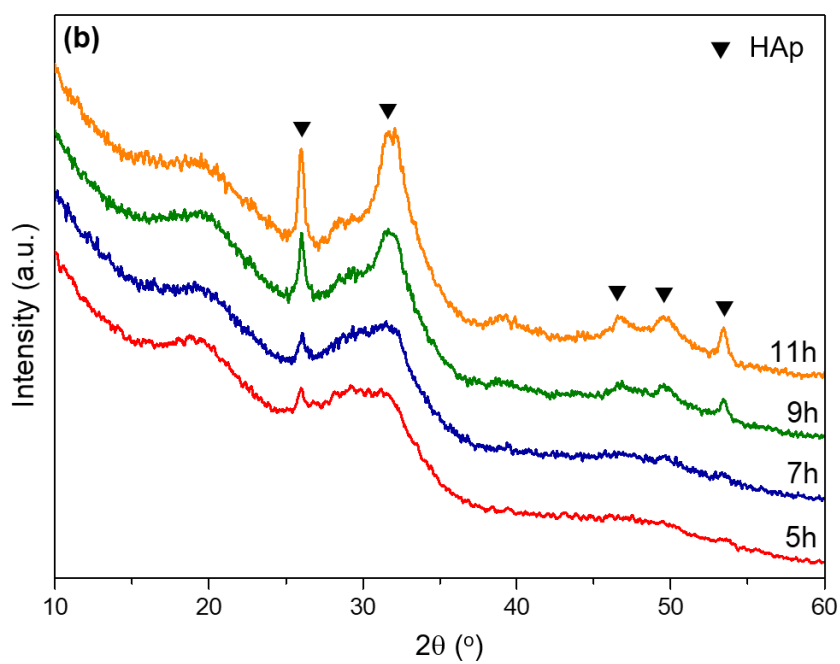
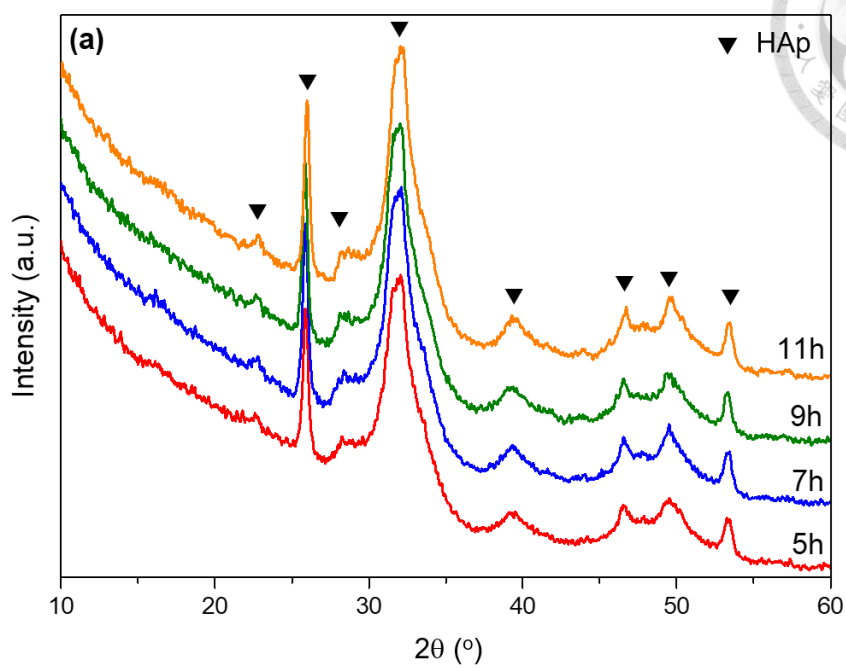


Figure 4.2 The XRD pattern of HAp and HAp-PC



Specifically, the conditions of HAp (Ca/Mg=5) are performed in the solution environment and physiological temperature at 37 °C to track the transformation from ACP to HAp with increasing aging time. Comparison with the crystallization process of the HAp (Ca/Mg=5) with and without the different amounts of PC molecules are shown in **Figure 4.3**. It significantly shows that the PC used system has lower crystallinity. At the aging time of 5 hours, the PC-assisted mineral can sustain the amorphous phase of the calcium phosphate, which shown in **Figure 4.3 (b)**. Additionally, using larger amount of the PC to synthesize the material could extend the state of the amorphous phase for at least 11 hours (**Figure 4.3 (c)**). However, the transformation of the ACP to HAp occurred at the 5 hours aging time in the control experiment if the PC was not used. Thus, the addition of the PC affects crystallinity and the time of the crystallization process for HAp.



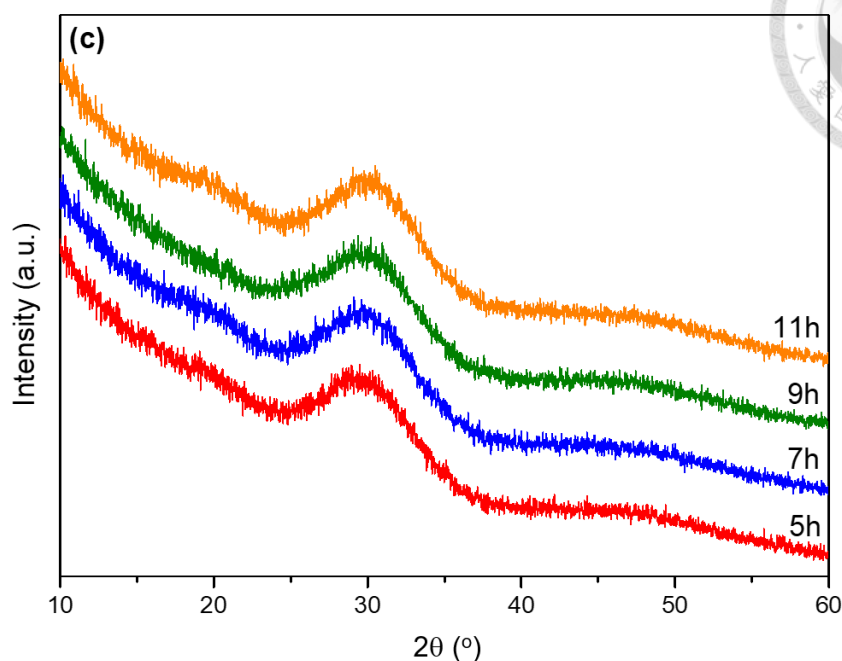


Figure 4.3 The XRD comparison of (a) the different aging time of the HAp (Ca/Mg=5), (b) HAp-PC (Ca/Mg=5) and (c) HAp-1.5PC (Ca/Mg=5) crystallization

As shown in **Figure 4.4**, there is almost no difference in the results of XRD between HAp and HAp-PC (Ca/Mg=5). To verify this crystal alignment phenomenon, high resolution TEM of HAp without and with PC confinement are performed to observe the difference of the crystal orientation in **Figure 4.5**. As shown in **Figure 4.5 (a) and (c)**, polycrystalline is observed with the selected area electron diffraction (SAED) for HAp (Ca/Mg=5) and HAp-PC (Ca/Mg=5). Accordingly, the (211) diffraction pattern belonging to the characteristic peak of HAp appears at 31.86° in the XRD of **Figure 4.4** and are also observed with the SAED. Compared with the HAp, the intensity of the diffraction pattern

is weaker for HAp-PC (Ca/Mg=5). It is supposed that the PC provides the confined space and inhibits the crystallization process. The crystallinity is lower in the PC system than the system in absence of PC.

The dark-field images originating from the (211) diffraction spots are recorded in **Figure 4.5 (b) and (d)**, which is the morphology region from the bright field image in **Figure 4.5 (a) and (c)**, respectively. The bright spots show the crystal distribution of HAp, and the line connected by the bright spots indicates the crystal plane grows in the same direction. But only HAp-PC (Ca/Mg=5) have orderly arrangement under nanoscale. It aligned to form the bundle-like morphology in which the length size is around 300 nm. It is indicated that the formation of the orderly alignment is attributed to the function of organic matrix⁴⁶. This phenomenon is similar to the crystal arrangement of biological bone^{47, 48}.

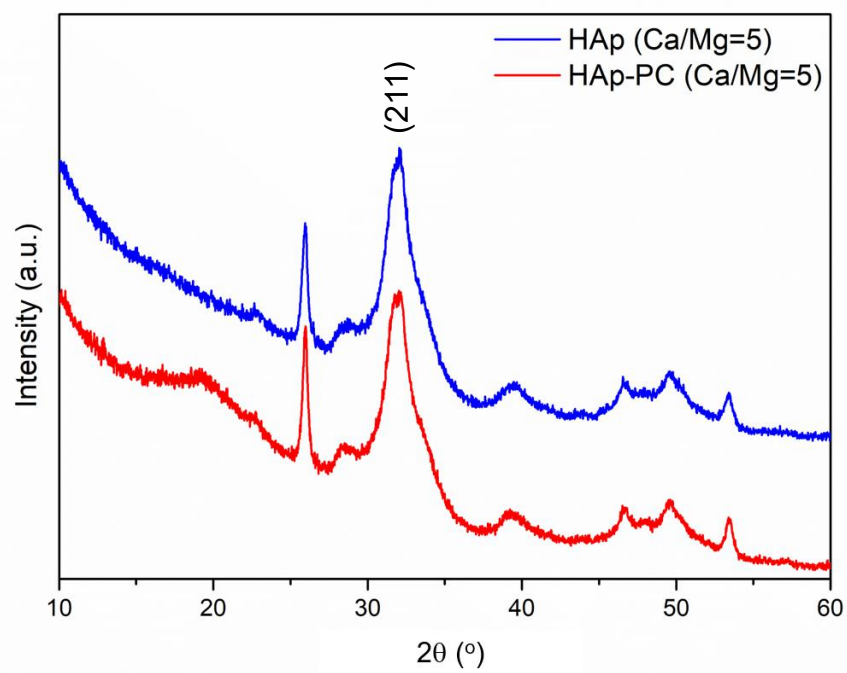


Figure 4.4 The XRD pattern of HAp (Ca/Mg=5) and HAp-PC (Ca/Mg=5)

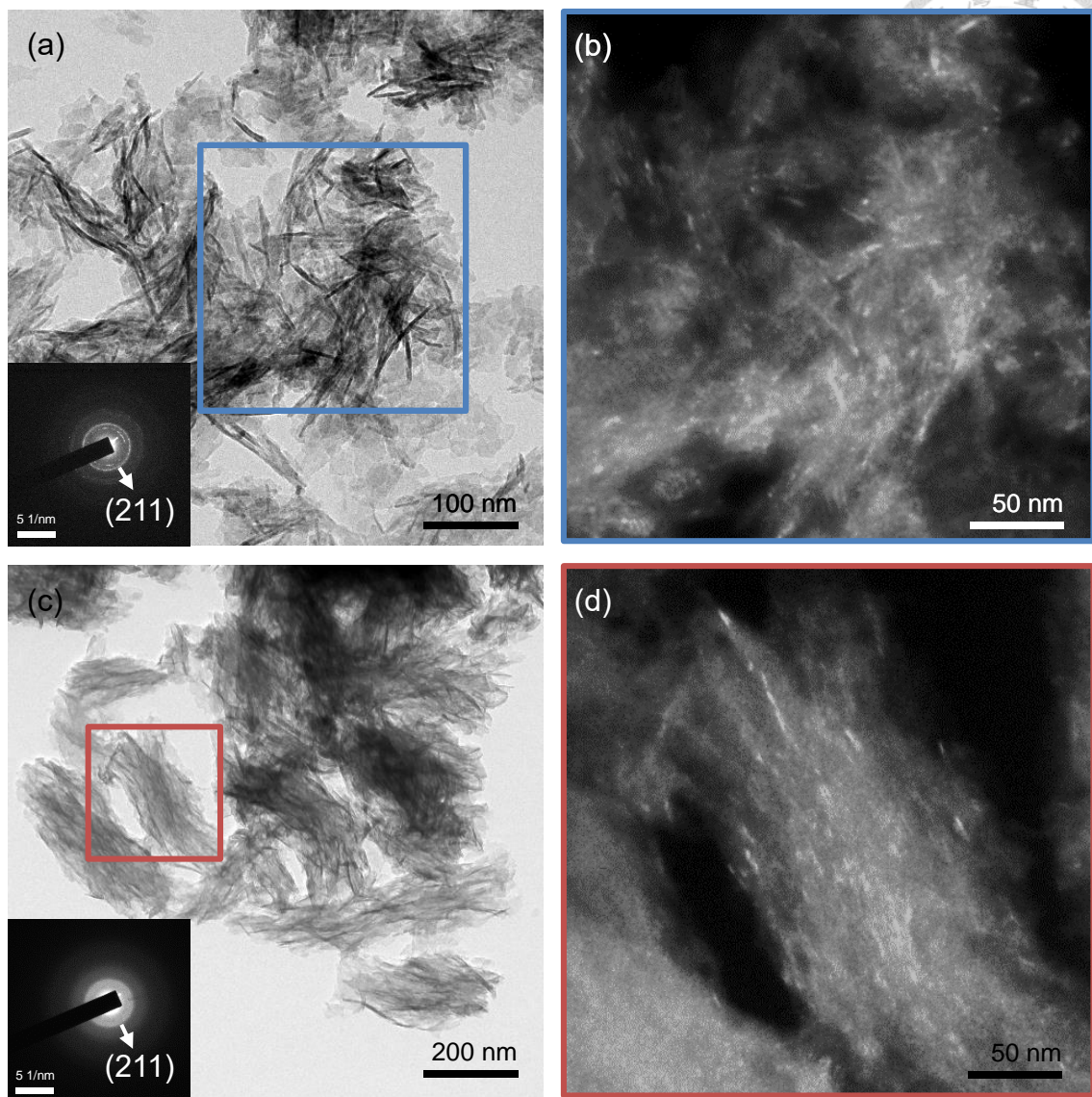



Figure 4.5 The TEM image of (a)(b) HAp (Ca/Mg=5) and (c)(d) HAp-PC (Ca/Mg=5)



The different Ca/Mg ratio of the solution is used to modulate the Mg content of the HAp (Ca/Mg=x) (x=10, 5, 1) in the aging 19 hours condition. The results of XRD show in **Figure 4.6** reveal the crystallinity decreases with the increase of the ratio of the Mg/Ca. The decrease of the crystallinity is caused by the Mg ions which could inhibit the crystallinity in HAp.⁴⁹ Furthermore, comparing with the HAp-PC (Ca/Mg=10), the corresponding peaks of HAp-PC (Ca/Mg=5) shift to the higher degree, owing to the increase of Mg replacement in HAp.

The morphology of the Mg@HAp and Mg@HAp-PC is observed with SEM in **Figure 4.7**. The shape morphology of HAp and HAp (Ca/Mg=10) is needle-like particles with agglomerated form; however, in the PC-incorporated system, the morphology is observed in the form of flakes. The morphology of HAp (Ca/Mg=5) with and without PC are compared in **Figure 4.7 (e) (f)**. It is shown that the irregular particle would aggregate and form the large crystal size in the control experiment (**Figure 4.7 (e)**). In the PC-incorporated system, the morphology appears to be bundle-like, which suggests the crystal axis might be aligned in the same direction to form a large ordered crystal, which is consistent with the TEM image in **Figure 4.5 (c)**. Especially, there are many large size columnar like morphologies in the high Mg content system for HAp (**Figure 4.7 (g)-(j)**). Both PC-incorporated and pure inorganic HAp (Ca/Mg=1) are in columnar morphology. However, the particle of the HAp-PC (Ca/Mg=1) is presented with the oriented array of

flake structure instead of the blocky in the pure inorganic HAp (Ca/Mg=1).

The zeta potential for Mg@HAp and Mg@HAp-PC are shown in **Figure 4.8**, and all of the samples for zeta potential analysis value are negative. In the condition of adding PC for the same ratio of Ca/Mg, the zeta potential can be lower than at least 2 times compared without PC condition, and the minimum zeta potential value is -25.83 mV which is observed from HAp-PC (Ca/Mg=1). The lower zeta potential of the material containing PC can be attributed to the pure PC having a large negative zeta potential. There are also several studies reporting negative zeta potential value for HAp and other bioceramics. The negative potential of the material can promote the adsorption of calcium ions which will participate in the deposition of extracellular matrix required for cell attachment.^{50, 51} Because the negative zeta potential has a beneficial effect on attachment and proliferation for bone cells which has been demonstrated^{52, 53}, the HAp-PC are believed to promote the bioactivity.

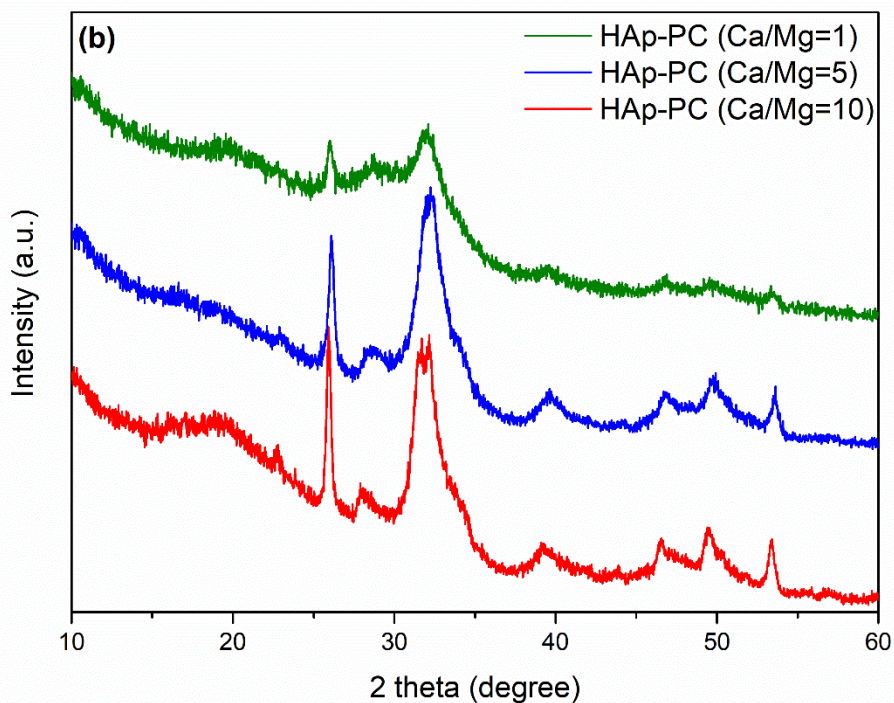
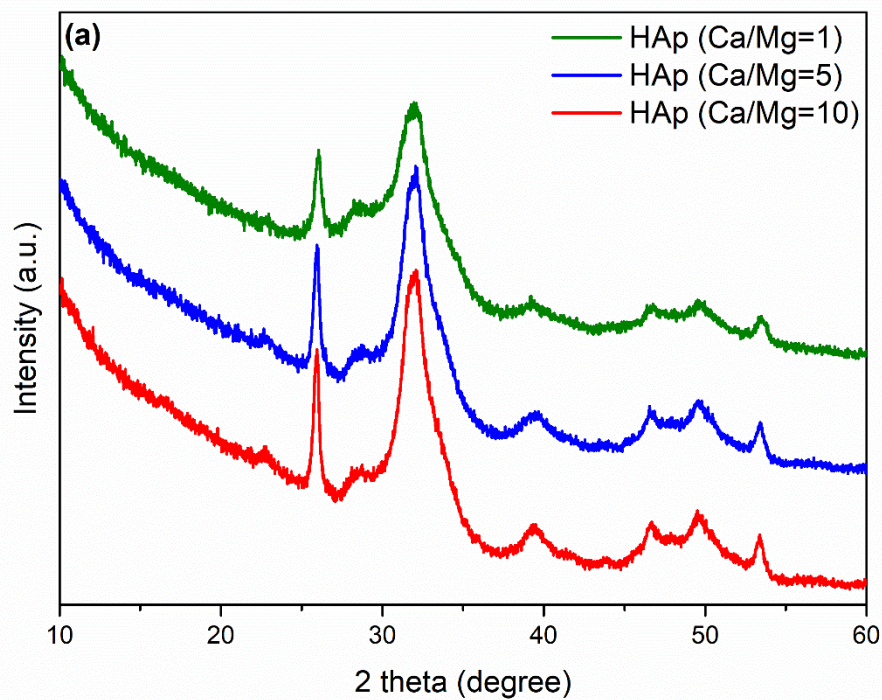
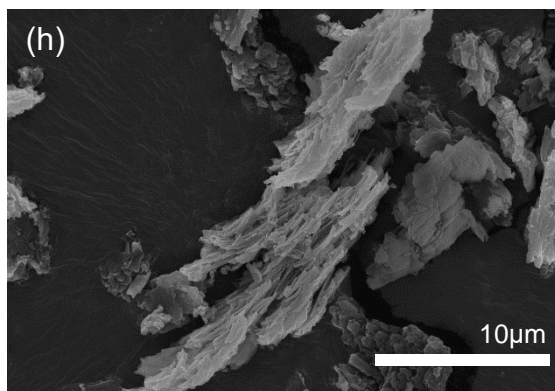
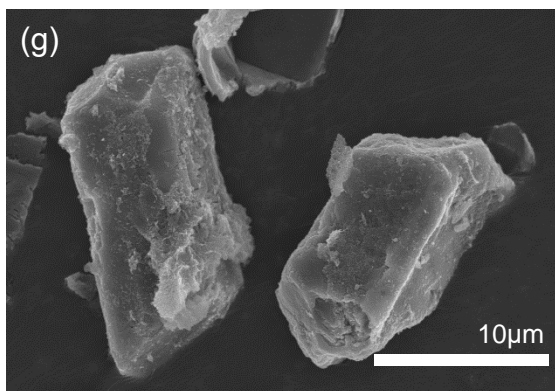
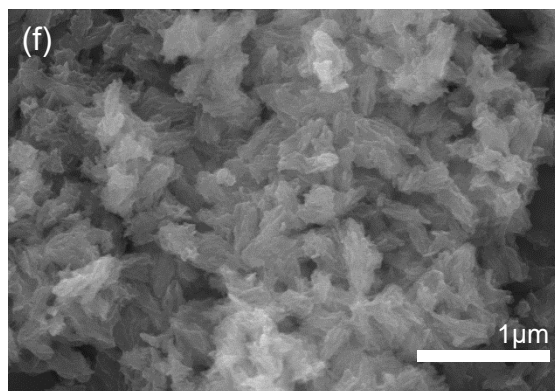
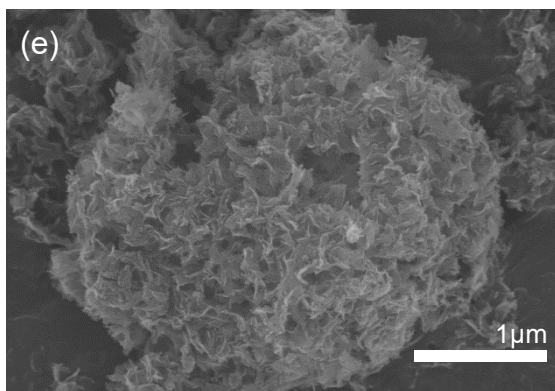
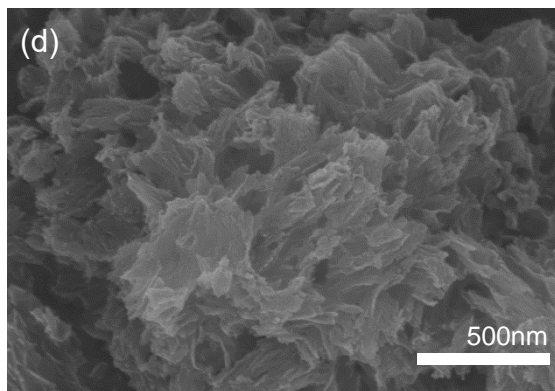
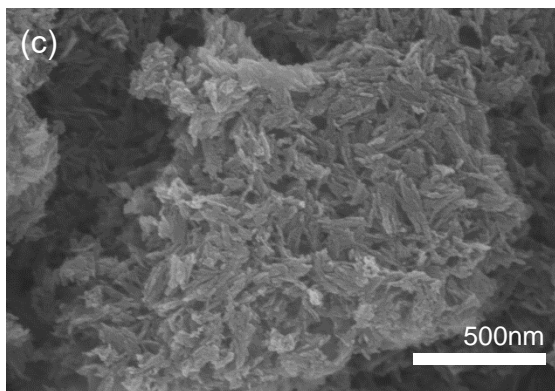
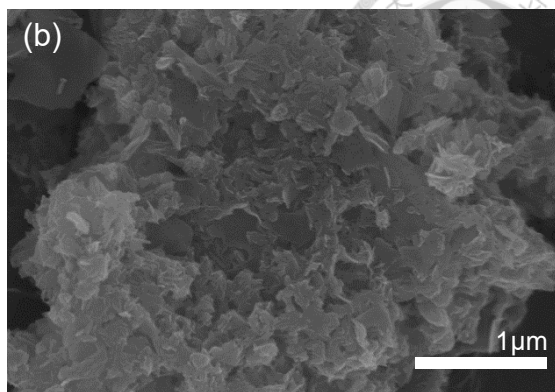
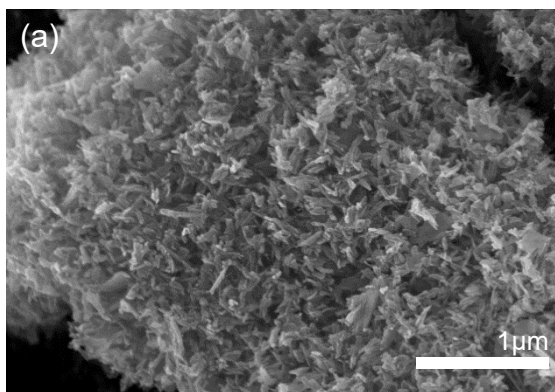


Figure 4.6 The XRD pattern of (a) HAp (Ca/Mg=10), HAp (Ca/Mg=5) and HAp (Ca/Mg=1) (b) HAp-PC (Ca/Mg=10), HAp-PC (Ca/Mg=5) and HAp-PC (Ca/Mg=1)



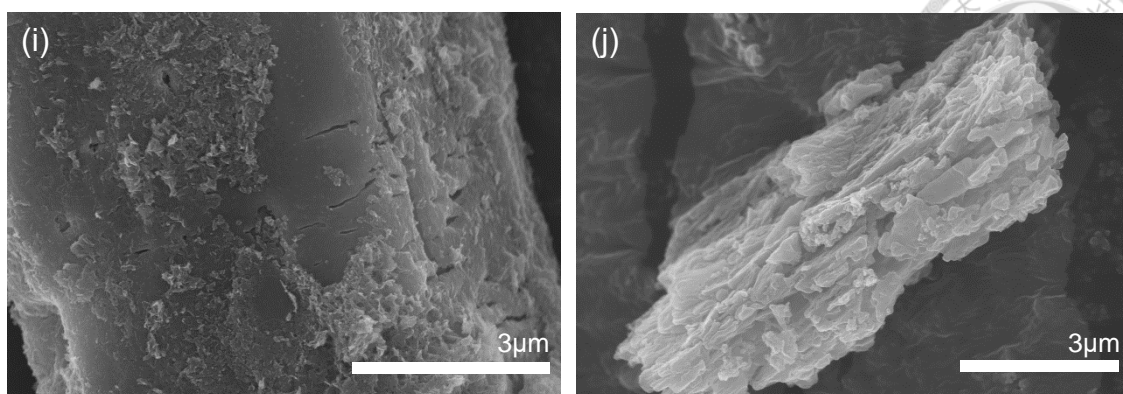


Figure 4.7 SEM image of (a) HAp (b) HAp-PC (c) HAp (Ca/Mg=10) (d) HAp-PC (Ca/Mg=10) (e) HAp (Ca/Mg=5) (f) HAp-PC (Ca/Mg=5) (g)(i) HAp (Ca/Mg=1) (h)(j)

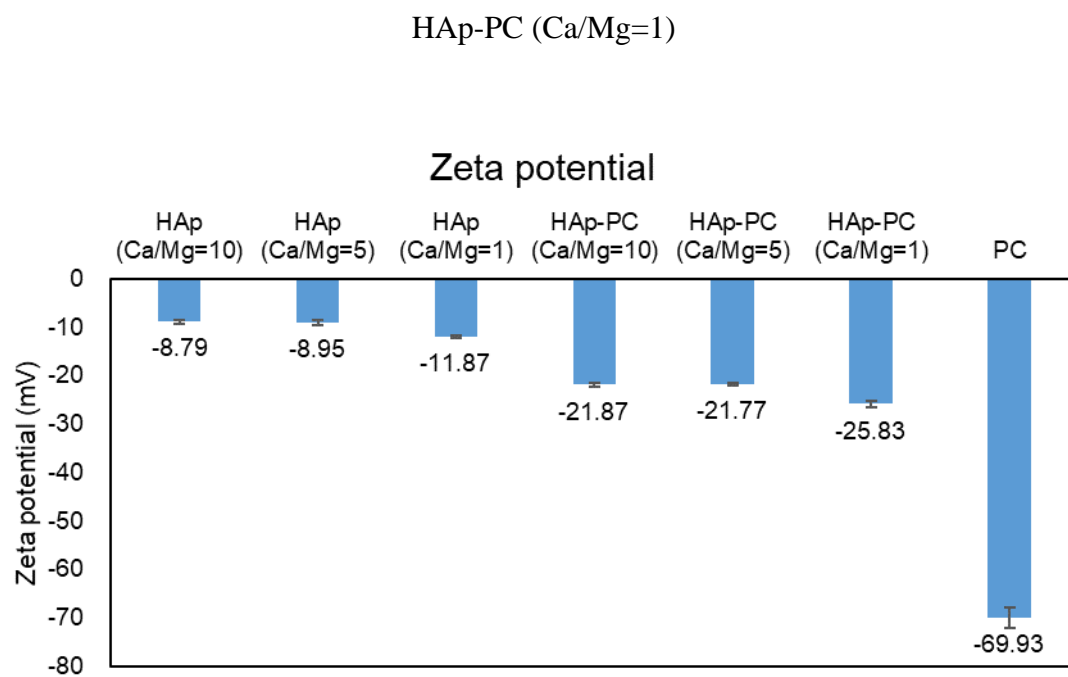
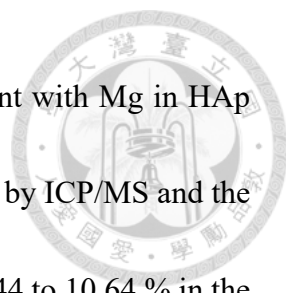
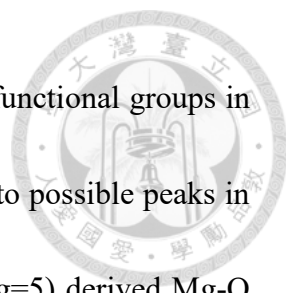


Figure 4.8 Zeta potential of Mg@HAp, Mg@HAp-PC, and PC



To demonstrate the Mg content and the Ca amount replacement with Mg in HAp and HAp-PC, the Ca and Mg contents for each sample were detected by ICP/MS and the results are shown in **Table 4.1**. Mg content can be controlled from 1.44 to 10.64 % in the PC system. To better evaluate the change of composition in each sample, we normalize the product molar ratio and calculated the percentage of Ca replacement with Mg and the ratio of Ca/Mg. It is confirmed that with the use of PC, it is possible to increase the proportion of Ca replacement with Mg or the amount of Mg-loaded. This is attributed to the addition of PC can increase the stability of Mg in HAp, which will be verified by reaction mechanism.

As mentioned in **section 1.3**, usually, the incorporation of Mg in synthetic HAp is limited, which is the maximum of about 0.4 wt%²⁴. It is difficult to prepare a high Mg contained HAp in aqueous solution at physiological temperature. The reason is because the hydration energy of the Mg in the aqueous environment is too high to incorporate the Mg in the mineral crystal structure²³, unless other ions, such as carbonate or fluoride are incorporated together with Mg as substitutions. However, the Mg@HAp materials have been successfully prepared by the PC molecules at physiological temperature in this research. In order to confirm how Mg is incorporated in HAp, the chemical state of magnesium and oxygen is identified with XPS (**Figure 4.10**). The signals in the Mg2p spectra are detected on the surfaces which support the presence of Mg. We use FTIR



spectrum of HAp and HAp-PC (Ca/Mg=5) (**Figure 4.9**) to analyze functional groups in materials. The results are the same as in **Figure 4.1** and correspond to possible peaks in the XPS spectrum. The chemical state of HAp and HAp-PC (Ca/Mg=5) derived Mg-O from carbonate (red line) shows the peak belonged to Mg2p with Mg^{2+} peak around 51.9 eV⁵⁴, which is in accordance with the results obtained from the O1s spectra. HAp-PC has 6 % Mg binding with carbonate, less than 16 % that HAp has. Some studies indicated that carbonates replace the phosphate ions in the crystal structure and have an impact on the ability of the structure to accommodate other foreign ions⁵⁵. Therefore, this result can provide the reason for high Mg content in HAp-PC is not completely attributed to carbonate. It is indirectly explained that Mg content increased mainly by the assistance of PC instead of carbonate for the HAp-PC.

As shown in O1s spectra, it could be observed the binding energy at 534.8 eV and 536.5 eV which might be respectively assigned to PO_4^{3-} and adsorbed water⁵⁶⁻⁵⁸. Additionally, a peak observed at 532.2 eV in HAp (Ca/Mg=5) is attributed to CO_3^{2-} bond⁵⁹. Furthermore, the binding energy of 532.1 eV and 534.4 eV may be attributed to ester C=O and O=C-O⁶⁰, respectively, and the existence of PC is also confirmed.

Table 4.1 ICP/MS of Mg@HAp and Mg@HAp-PC

Sample	Mg	Ca replacement with Mg	Ca/Mg
	(wt%)	Mg/(Mg+Ca) (%)	(-)
HAp (Ca/Mg=10)	1.48	8.02	11.48
HAp-PC (Ca/Mg=10)	1.44	8.77	10.40
HAp (Ca/Mg=5)	2.48	13.37	6.48
HAp-PC (Ca/Mg=5)	2.58	16.08	5.22
HAp (Ca/Mg=1)	8.36	41.98	1.38
HAp-PC (Ca/Mg=1)	10.64	44.73	1.24

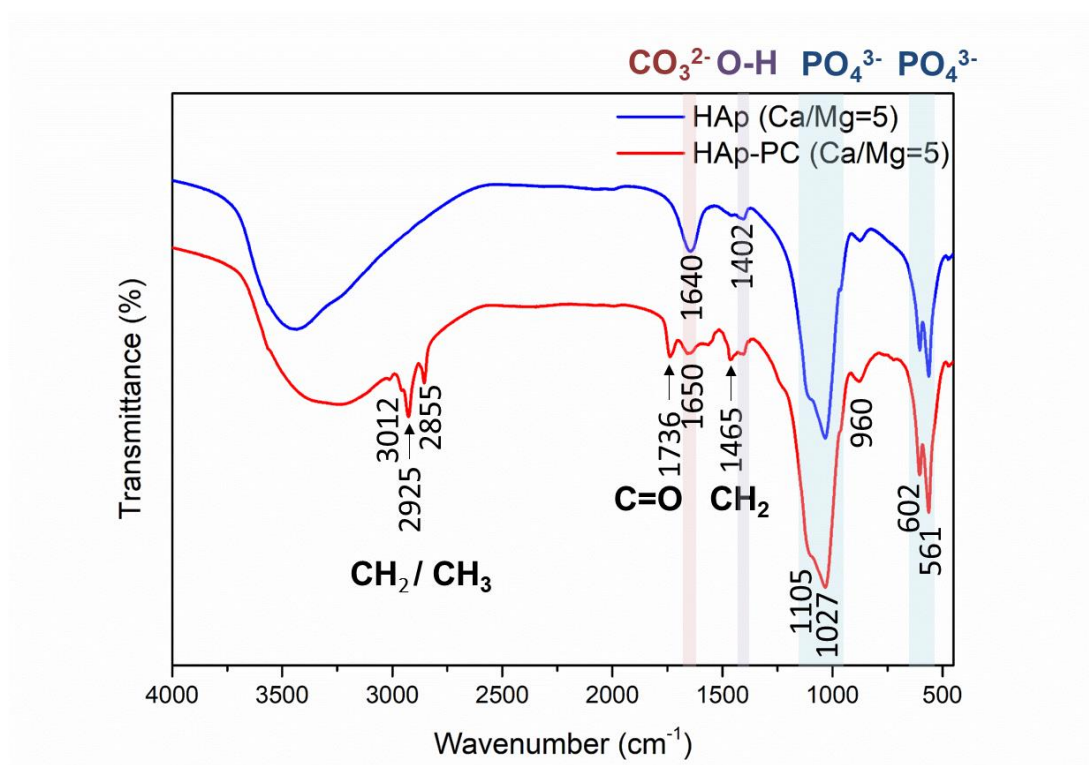


Figure 4.9 FTIR analysis of HAp and HAp-PC (Ca/Mg=5)

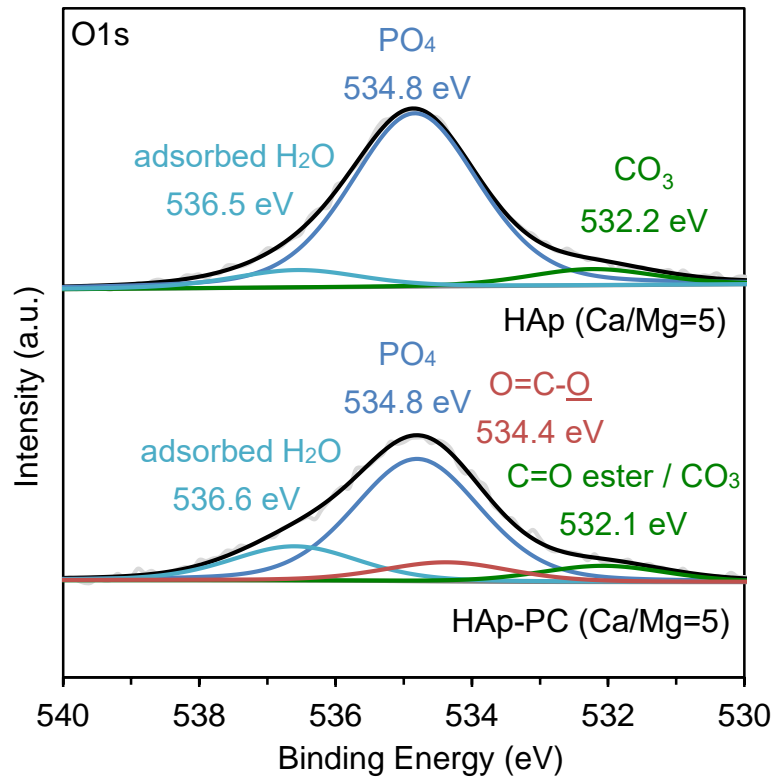
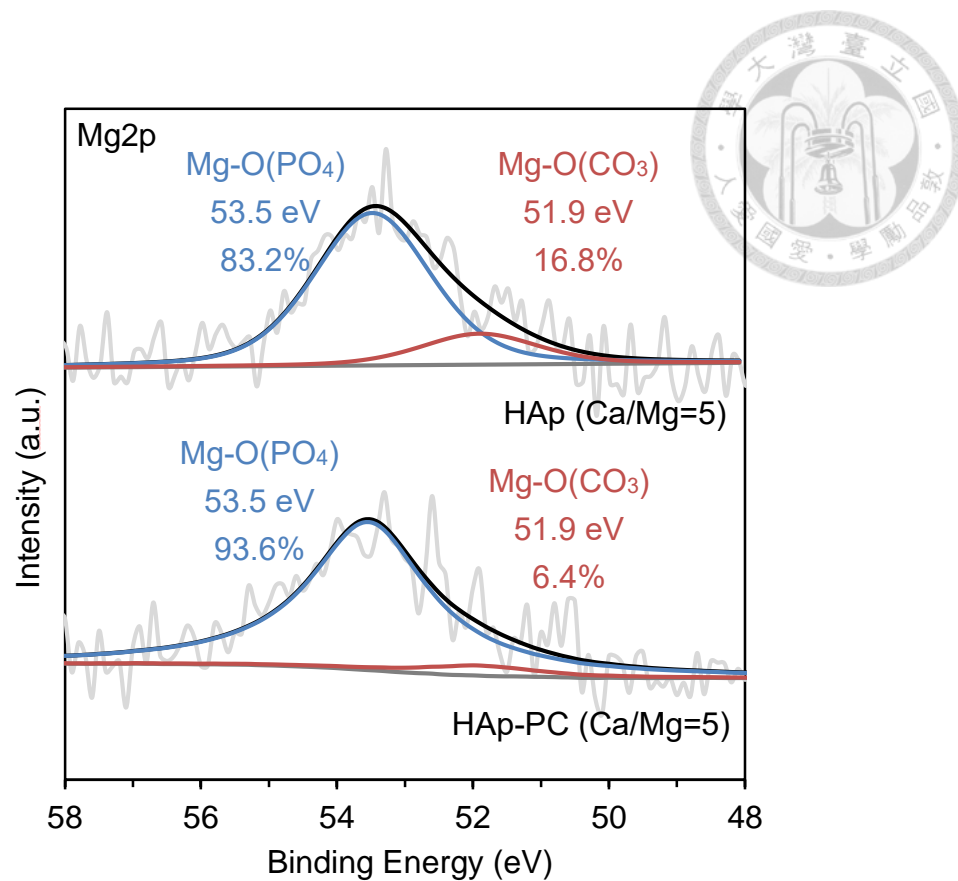


Figure 4.10 XPS analysis of HAp and HAp-PC (Ca/Mg=5)

4.2. PC-assisted reaction mechanism



In this section, how the Mg increased by the assistance of PC is investigated. It is predicted that the mechanism of PC-assisted synthesis is to adsorb Mg ions by the surface of the liposome vesicles (**Figure 4.11**). The Ca and Mg solution are mixed with PC and will be adsorbed on the PC vesicles at the same time. When the phosphate solution is added, the PC provides a stable nucleation space between Ca, Mg ions and phosphate ions and offer Mg ions to accommodate in HAp. Therefore, in order to prove this mechanism, the experiment process is modified. The experiment process differs from the order for the addition of calcium and magnesium solutions. As shown in **Figure 4.12**, the modified process is first mixing with calcium solution and PC for 30 minutes. This procedure is to let calcium ions adsorb to liposome vesicles totally. When adding the Mg solution, there is basically no space on the liposome vesicles to adsorb Mg ions. While adding dropwise phosphate solution, Mg ions cannot stably nucleation in HAp by the support of PC. The results obtained here also indicates that for the condition of Ca-occupied PC, the amount of Ca replacement with Mg indeed decreases to 14.28 %. It is achieved the expected results and also confirms this mechanism.

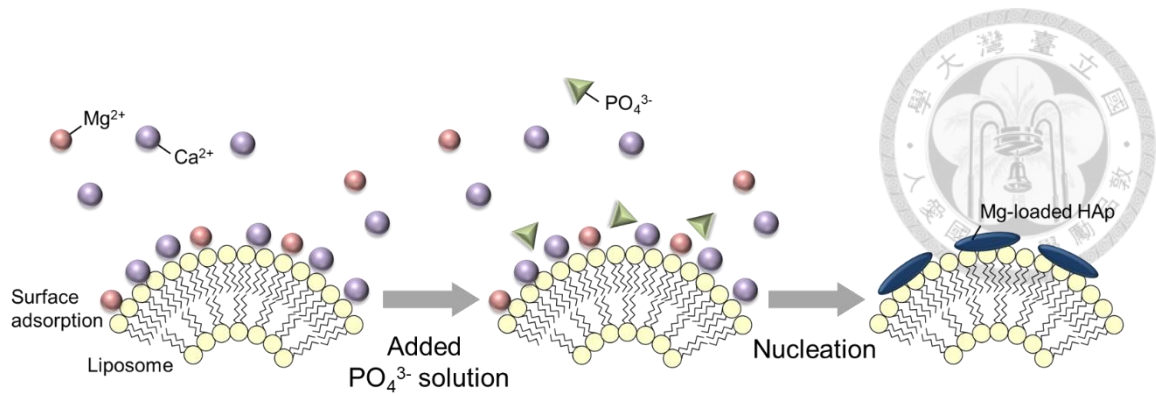


Figure 4.11 Principle of the nucleation on the surface of liposome vesicles in the reaction synthesized

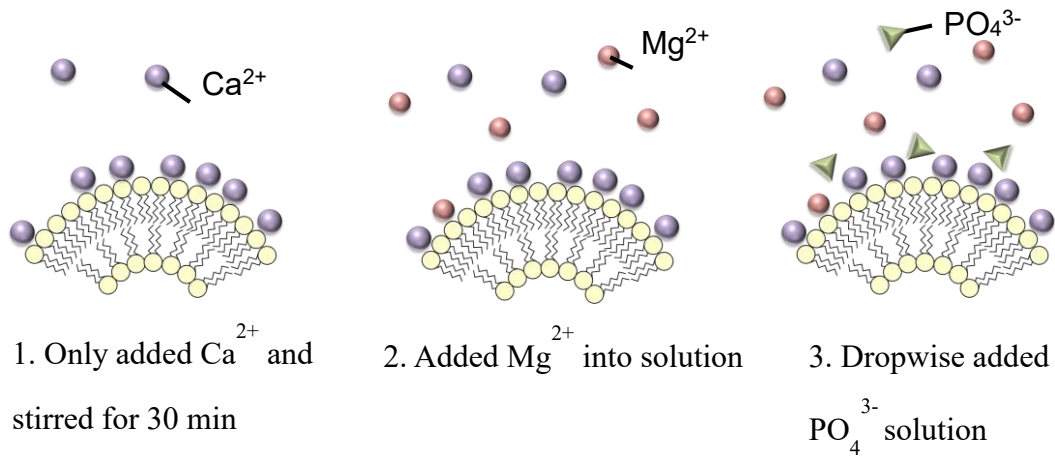



Figure 4.12 Process for preparing HAp-Ca occupied PC (Ca/Mg=5)

Table 4.2 ICP/MS of Mg@HAp-PC in different process



Sample	ICP	
	Ca replacement with Mg	Ca/Mg
	Mg/(Mg+Ca) (%)	(-)
HAp-PC (Ca/Mg=5)	16.08	5.22
HAp-Ca occupied PC (Ca/Mg=5)	14.28	6.00



4.3. Degradation test

To determine the degradation behavior of HAp and HAp-PC powder, the weight change for various time periods was examined. The *in vitro* biodegradation of the different Ca/Mg ratio of HAp and HAp-PC after 4 weeks of immersion in PBS is represented in **Figure 4.13**. The degradation rate of samples could be controlled from 9.43 to 28.06 % in 4 weeks. For the same ratio of Ca to Mg, the addition of PC significantly increases the degradation rate of the HAp. Higher concentration of Mg in the HAp also increases the degradation rate. The main effect of the increase in degradation rate is the Mg content in HAp, which is consistent with the early study^{15, 24}. In addition, the controllable degradation rate maybe matches the rate of new bone formation.

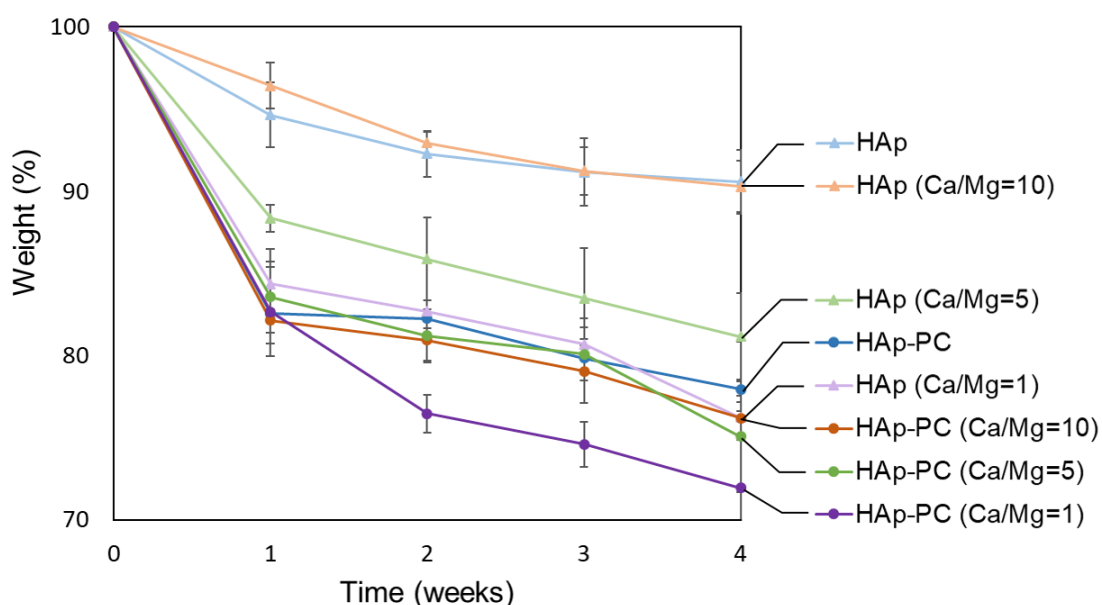


Figure 4.13 Degradation of Mg@HAp and Mg@HAp-PC for various time periods

4.4. *In vitro* test

4.4.1. Cell viability and proliferation



To detect the biocompatibility of materials, various concentrations of Mg@HAp and Mg@HAp-PC particles are added into the culture medium of MG63 cell line. The MTT assay of MG63 cell for cytotoxicity result in 1 day is shown in **Figure 4.14**. All the materials have good biocompatibility that the cell viability is above 80% for different concentration after 1 day. Especially for HAp-PC (Ca/Mg=1) in 10 mg/mL, the cell viability can be as high as 221%, which is supposed to the release of high concentration of Mg ions. Although the HAp-PC (Ca/Mg=1) in 10 mg/mL has the best effect for cell viability, the other samples are the opposite. Therefore, we used 1 mg/mL as the appropriate concentration of cell proliferation test in the 3, 5, 7 and 14 days of culture (**Figure 4.15**). The result shows that the HAp-PC have higher cell viability compared with HAp. And the cell viability of all materials is outstandingly different from the control group after 2 weeks. In addition, HAp-PC (Ca/Mg=5) and HAp-PC (Ca/Mg=1) have significant differences after the 5th day. It indicates that the presence of high Mg content in HAp and addition of PC are beneficial to cellular proliferation.

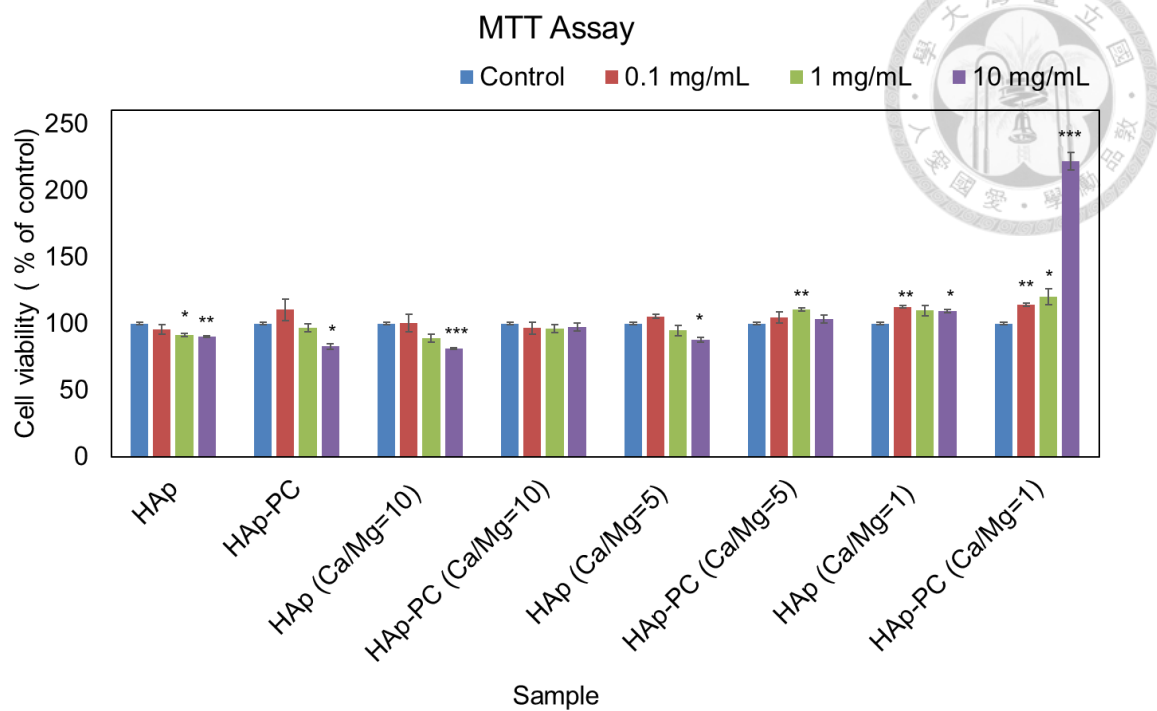


Figure 4.14 Cytotoxicity of various concentrations of Mg@HAp and Mg@HAp-PC in 1 day of culture

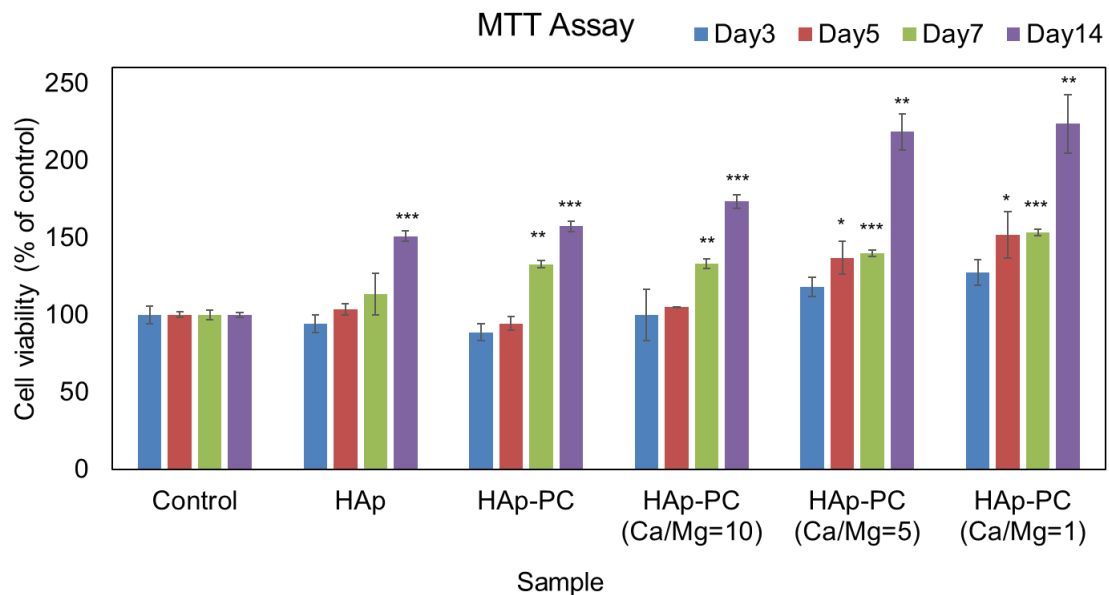
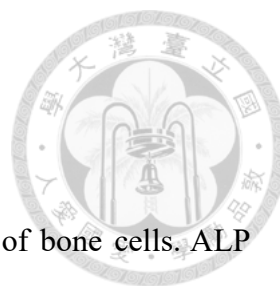


Figure 4.15 Proliferation assay of HAp and Mg@HAp-PC



4.4.2. Cellular differentiation

ALP activity is often used to demonstrate the differentiation of bone cells. ALP activity increases when bone cells undergo the mineralization process. The ALP concentrations of HAp and Mg@HAp-PC after 3, 5, 7 and 14 days are shown in **Figure 4.16**. It shows that the ALP concentration of all treatment group which immersed material continued to rise during 14 days and performed better than the control group. Especially in the case of HAp-PC (Ca/Mg=1) is 97% higher than the control group after 14 days. It can be determined that the bone cells had entered the stage of mineralization and the Mg@HAp-PC can promote the differentiation of osteoblasts.

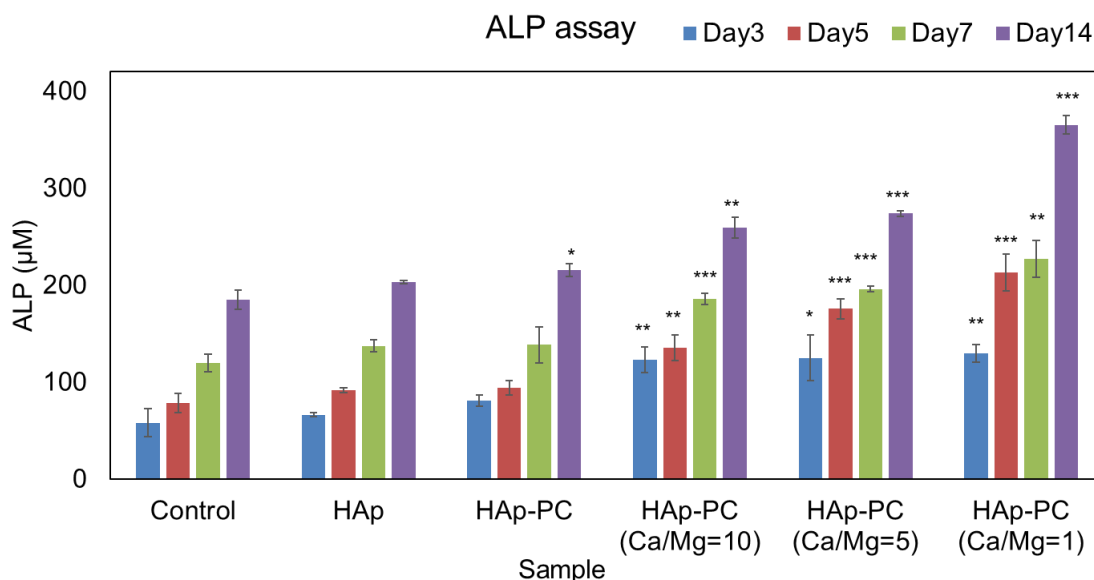
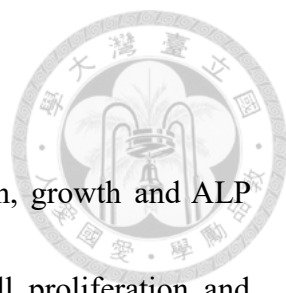


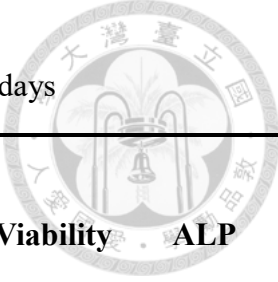
Figure 4.16 Differentiation assay of HAp and Mg@HAp-PC

4.4.3. Quantitative analysis of Mg ions release



It has been demonstrated that Mg ions can increase adhesion, growth and ALP activity of bone cell¹⁴. To investigate the causes of increased cell proliferation and differentiation, we analyze the release concentration from the material and cell uptake of magnesium ion after 3 days. Because the best bioactivity effect of the ratio of Ca to Mg is 1, we use this ratio to examine. In the previous results (**Table 4.1**), it has been considered that the higher Mg content of HAp can be synthesized with the aid of PC. From **Table 4.3**, we can indicate the released 0.89 wt% of Mg ions for HAp-PC(Ca/Mg=1) in 3 days, which is higher than 0.74 wt% of HAp (Ca/Mg=1). The Mg ions intake of the cells is 0.12 and 0.14 wt% for HAp and HAp-PC (Ca/Mg=1), respectively. As a consequence, it showed that when the Mg ions release and the concentration increased, the viability and ALP concentration increased. This phenomenon which benefits cell proliferation and differentiation is mainly caused by the concentration of Mg ion release.

Table 4.3 The Mg ions release and uptake of cell in 3 days



Sample	Mg	Release of Mg ²⁺	Mg ²⁺ uptake of cell	Viability	ALP
	(wt %)	(wt %)	(wt %)	(% of control)	
HAp (Ca/Mg=1)	8.36	0.74±0.04	0.12±0.05	107.92	170.75
HAp-PC (Ca/Mg=1)	10.64	0.89±0.06	0.14±0.09	127.53	222.55
Data represent the mean SD for three replicates					

5. Conclusion



We had successfully synthesized Mg@HAp for the Ca/Mg ratio of 10, 5, 1 with the assistance of PC. The addition of the PC effects crystallinity and the time of the crystallization process for HAp. Moreover, it is indicated that the formation of the orderly crystal alignment is attributed to the presence of PC organic matrix. PC provides the stability of Mg in HAp and increases the loading amount of Mg, that the content of Mg being controllable from 1.44 to 10.64 wt%. Increasing the content of Mg in HAp mainly by the assistance of PC instead of carbonate has been confirmed. The proposed mechanism indicates PC provides a stable nucleation space between Ca, Mg and phosphate ions and offer Mg ions to accommodate in HAp. The degradation rate for Mg@HAp could be controlled in range of 9.71 to 28.06 % in 4 weeks. The primary effect of degradation rate is the Mg content in HAp; increasing Mg content resulted in higher degradation rate. For *in vitro* test, there is 0.89 wt% Mg ions release from HAp-PC (Ca/Mg=1) leading to 127% cellular viability and 222% ALP concentration after 3 days. The presence of high Mg and addition of PC in HAp are beneficial to cellular proliferation and differentiation, and the release of Mg ions is major factors for promotion. Consider all, this work reveals a novel efficacy for PC applied in Mg@HAp, and provide a promising biomaterial in orthopedic applications.

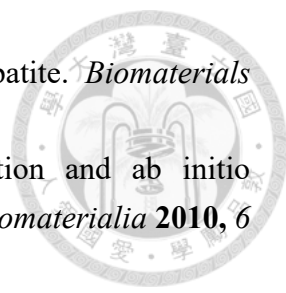
6. Future Prospects

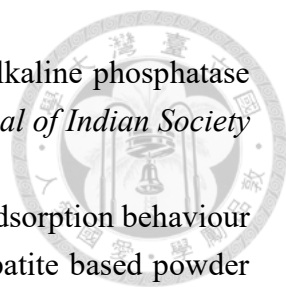
Mg@HAp by PC-assisted synthesis is a potential material for bone filler. Besides the form of powder, it can be applied in blending with polymer as a composite material to improve its mechanical properties. In the future, we can perform RT-PCR assay to confirm the relevant osteoblasts gene expression and *in vivo* experiments.

7. Reference

1. Dimitriou, R., Jones, E., McGonagle, D., Giannoudis, P. V., Bone regeneration: current concepts and future directions. *Bmc Medicine* **2011**, 9, 10.
2. Einhorn, T. A., The cell and molecular biology of fracture healing. *Clinical Orthopaedics and Related Research* **1998**, 355, S7-S21.
3. O'Brien, F. J., Biomaterials & scaffolds for tissue engineering. *Materials Today* **2011**, 14 (3), 88-95.
4. Atala, A., Tissue engineering and regenerative medicine: Concepts for clinical application. *Rejuvenation Research* **2004**, 7 (1), 15-31.
5. Stevens, M. M., Biomaterials for bone tissue engineering. *Materials Today* **2008**, 11 (5), 18-25.
6. Burg, K. J. L., Porter, S., Kellam, J. F., Biomaterial developments for bone tissue engineering. *Biomaterials* **2000**, 21 (23), 2347-2359.
7. Rezwan, K., Chen, Q. Z., Blaker, J. J., Boccaccini, A. R., Biodegradable and bioactive porous polymer/inorganic composite scaffolds for bone tissue engineering. *Biomaterials* **2006**, 27 (18), 3413-3431.
8. Sadat-Shojai, M., Khorasani, M.-T., Dinpanah-Khoshdargi, E., Jamshidi, A., Synthesis methods for nanosized hydroxyapatite with diverse structures. *Acta Biomaterialia* **2013**, 9 (8), 7591-7621.
9. Berzina-Cimdina, L., Borodajenko, N., Research of calcium phosphates using Fourier transform infrared spectroscopy. In *Infrared Spectroscopy-Materials Science, Engineering and Technology*, IntechOpen: 2012.
10. Hannink, G., Arts, J. C., Bioresorbability, porosity and mechanical strength of bone substitutes: what is optimal for bone regeneration? *Injury* **2011**, 42, S22-S25.
11. Galia, C. R., Lourenço, A. L., Rosito, R., Souza Macedo, C. A., Camargo, L. M. A. Q., PHYSICOCHEMICAL CHARACTERIZATION OF LYOPHILIZED BOVINE BONE GRAFTS. *Revista Brasileira de Ortopedia (English Edition)* **2011**, 46 (4), 444-451.
12. Gozalian, A., Behnamghader, A., Daliri, M., Moshkforoush, A., Synthesis and thermal behavior of Mg-doped calcium phosphate nanopowders via the sol gel method. *Scientia Iranica* **2011**, 18 (6), 1614-1622.
13. Zilm, M., Chen, L., Sharma, V., McDannald, A., Jain, M., Ramprasad, R., Wei, M., Hydroxyapatite substituted by transition metals: experiment and theory. *Physical Chemistry Chemical Physics* **2016**, 18 (24), 16457-16465.
14. Liangzhi, G., Weibin, Z., Yuhui, S., Magnesium substituted hydroxyapatite whiskers: synthesis, characterization and bioactivity evaluation. *RSC Advances*

- 2016**, 6 (115), 114707-114713.
15. Zhang, Y. F., Xu, J. K., Ruan, Y. C., Yu, M. K., O'Laughlin, M., Wise, H., Chen, D., Tian, L., Shi, D. F., Wang, J. L., Chen, S. H., Feng, J. Q., Chow, D. H. K., Xie, X. H., Zheng, L. Z., Huang, L., Huang, S., Leung, K., Lu, N., Zhao, L., Li, H. F., Zhao, D. W., Guo, X., Chan, K. M., Witte, F., Chan, H. C., Zheng, Y. F., Qin, L., Implant-derived magnesium induces local neuronal production of CGRP to improve bone-fracture healing in rats. *Nature Medicine* **2016**, 22 (10), 1160-1169.
 16. Willumeit, R., Fischer, J., Feyerabend, F., Hort, N., Bismayer, U., Heidrich, S., Mihailova, B., Chemical surface alteration of biodegradable magnesium exposed to corrosion media. *Acta Biomaterialia* **2011**, 7 (6), 2704-2715.
 17. Landi, E., Logroscino, G., Proietti, L., Tampieri, A., Sandri, M., Sprio, S., Biomimetic Mg-substituted hydroxyapatite: from synthesis to in vivo behaviour. *Journal of Materials Science: Materials in Medicine* **2008**, 19 (1), 239-247.
 18. Myers, H., Calcium phosphates in oral biology and medicine. *Monographs in oral science* **1991**, 15.
 19. Jahnen-Dechent, W., Ketteler, M., Magnesium basics. *Clinical kidney journal* **2012**, 5 (Suppl_1), i3-i14.
 20. Chaudhry, A. A., Goodall, J., Vickers, M., Cockcroft, J. K., Rehman, I., Knowles, J. C., Darr, J. A., Synthesis and characterisation of magnesium substituted calcium phosphate bioceramic nanoparticles made via continuous hydrothermal flow synthesis. *Journal of Materials Chemistry* **2008**, 18 (48), 5900-5908.
 21. Lenders, J. J. M., Dey, A., Bomans, P. H. H., Spielmann, J., Hendrix, M., de With, G., Meldrum, F. C., Harder, S., Sommerdijk, N., High-Magnesian Calcite Mesocrystals: A Coordination Chemistry Approach. *Journal of the American Chemical Society* **2012**, 134 (2), 1367-1373.
 22. Bertoni, E., Bigi, A., Cojazzi, G., Gandolfi, M., Panzavolta, S., Roveri, N., Nanocrystals of magnesium and fluoride substituted hydroxyapatite. *Journal of Inorganic Biochemistry* **1998**, 72 (1-2), 29-35.
 23. Xu, J., Yan, C., Zhang, F., Konishi, H., Xu, H., Teng, H. H., Testing the cation-hydration effect on the crystallization of Ca-Mg-CO₃ systems. *Proceedings of the National Academy of Sciences of the United States of America* **2013**, 110 (44), 17750-17755.
 24. Suchanek, W. L., Byrappa, K., Shuk, P., Riman, R. E., Janas, V. F., TenHuisen, K. S., Preparation of magnesium-substituted hydroxyapatite powders by the mechanochemical-hydrothermal method. *Biomaterials* **2004**, 25 (19), 4647-4657.
 25. Laurencin, D., Almora-Barrios, N., de Leeuw, N. H., Gervais, C., Bonhomme, C., Mauri, F., Chrzanowski, W., Knowles, J. C., Newport, R. J., Wong, A., Gan,

- 
- Z.,Smith, M. E., Magnesium incorporation into hydroxyapatite. *Biomaterials* **2011**, 32 (7), 1826-1837.
26. Ren, F.,Leng, Y.,Xin, R.,Ge, X., Synthesis, characterization and ab initio simulation of magnesium-substituted hydroxyapatite. *Acta Biomaterialia* **2010**, 6 (7), 2787-2796.
 27. Cacciotti, I.,Bianco, A.,Lombardi, M.,Montanaro, L., Mg-substituted hydroxyapatite nanopowders: synthesis, thermal stability and sintering behaviour. *Journal of the European Ceramic Society* **2009**, 29 (14), 2969-2978.
 28. Fahy, E.,Subramaniam, S.,Brown, H. A.,Glass, C. K.,Merrill Jr, A. H.,Murphy, R. C.,Raetz, C. R.,Russell, D. W.,Seyama, Y.,Shaw, W., A comprehensive classification system for lipids. *European Journal of Lipid Science and Technology* **2005**, 107 (5), 337-364.
 29. Srour, B. Emerging roles for natural and artificial lipids in shaping the catalytic function, stability and oligomeric state of membrane proteins. Strasbourg, 2015.
 30. Huang, J.-S.,Liu, K.-M.,Chen, C.-C.,Ho, K.-Y.,Wu, Y.-M.,Wang, C.-C.,Cheng, Y.-M.,Ko, W.-L.,Liu, C.-S.,Ho, Y.-P., Liposomes-coated hydroxyapatite and tricalcium phosphate implanted in the mandibular bony defect of miniature swine. *The Kaohsiung Journal of Medical Sciences* **1997**, 13 (4), 213-228.
 31. Feng, Q.,Chen, Q.,Wang, H.,Cui, F., Influence of concentration of calcium ion on controlled precipitation of calcium phosphate within unilamellar lipid vesicles. *Journal of Crystal Growth* **1998**, 186 (1-2), 245-250.
 32. Chu, M.,Liu, G., Preparation and characterization of hydroxyapatite/liposome core-shell nanocomposites. *Nanotechnology* **2005**, 16 (8), 1208.
 33. Perttu, E. K.,Szoka, F. C., Zwitterionic sulfobetaine lipids that form vesicles with salt-dependent thermotropic properties. *Chemical Communications* **2011**, 47 (47), 12613-12615.
 34. Szcześ, A., Effects of DPPC/Cholesterol liposomes on the properties of freshly precipitated calcium carbonate. *Colloids and Surfaces B: Biointerfaces* **2013**, 101, 44-48.
 35. Lis, L.,Lis, W.,Parsegian, V.,Rand, R., Adsorption of divalent cations to a variety of phosphatidylcholine bilayers. *Biochemistry* **1981**, 20 (7), 1771-1777.
 36. Yu, P. T.,Tsao, C.,Wang, C. C.,Chang, C. Y.,Wang, C. H.,Chan, J. C. C., High-Magnesium Calcite Mesocrystals: Formation in Aqueous Solution under Ambient Conditions. *Angewandte Chemie* **2017**, 129 (51), 16420-16424.
 37. Kuete, V.,Karaosmanoğlu, O.,Sivas, H., Anticancer Activities of African Medicinal Spices and Vegetables. In *Medicinal Spices and Vegetables from Africa*, Elsevier: 2017; pp 271-297.

- 
38. Sanikop, S., Patil, S., Agrawal, P., Gingival crevicular fluid alkaline phosphatase as a potential diagnostic marker of periodontal disease. *Journal of Indian Society of Periodontology* **2012**, 16 (4), 513.
 39. Brundavanam, S., Poinern, G. E. J., Fawcett, D., Kinetic and adsorption behaviour of aqueous Fe²⁺, Cu²⁺ and Zn²⁺ using a 30 nm hydroxyapatite based powder synthesized via a combined ultrasound and microwave based technique. *American Journal of Materials Science* **2015**, 5 (2), 31-40.
 40. Nassif, N., Martineau, F., Syzgantseva, O., Gobeaux, F., Willinger, M., Coradin, T., Cassaignon, S., Azais, T., Giraud-Guille, M. M., In Vivo Inspired Conditions to Synthesize Biomimetic Hydroxyapatite. *Chemistry of Materials* **2010**, 22 (12), 3653-3663.
 41. Ren, F. Z., Ding, Y. H., Leng, Y., Infrared spectroscopic characterization of carbonated apatite: A combined experimental and computational study. *Journal of Biomedical Materials Research Part A* **2014**, 102 (2), 496-505.
 42. Destainville, A., Champion, E., Bernache-Assollant, D., Laborde, E., Synthesis, characterization and thermal behavior of apatitic tricalcium phosphate. *Materials Chemistry and Physics* **2003**, 80 (1), 269-277.
 43. Raynaud, S., Champion, E., Bernache-Assollant, D., Thomas, P., Calcium phosphate apatites with variable Ca/P atomic ratio I. Synthesis, characterisation and thermal stability of powders. *Biomaterials* **2002**, 23 (4), 1065-1072.
 44. Meejoo, S., Maneeprakorn, W., Winotai, P., Phase and thermal stability of nanocrystalline hydroxyapatite prepared via microwave heating. *Thermochimica Acta* **2006**, 447 (1), 115-120.
 45. Cagnasso, M., Boero, V., Franchini, M. A., Chorover, J., ATR-FTIR studies of phospholipid vesicle interactions with alpha-FeOOH and alpha-Fe₂O₃ surfaces. *Colloids and Surfaces B-Biointerfaces* **2010**, 76 (2), 456-467.
 46. Sturm, E. V., Colfen, H., Mesocrystals: structural and morphogenetic aspects. *Chemical Society Reviews* **2016**, 45 (21), 5821-5833.
 47. Schwarcz, H. P., McNally, E. A., Botton, G. A., Dark-field transmission electron microscopy of cortical bone reveals details of extrafibrillar crystals. *Journal of structural biology* **2014**, 188 (3), 240-248.
 48. Ziv, V., Wagner, H. D., Weiner, S., Microstructure-microhardness relations in parallel-fibered and lamellar bone. *Bone* **1996**, 18 (5), 417-428.
 49. LeGeros, R. Z., Calcium phosphate-based osteoinductive materials. *Chemical reviews* **2008**, 108 (11), 4742-4753.
 50. Cheng, K., Weng, W., Wang, H., Zhang, S., In vitro behavior of osteoblast-like cells on fluoridated hydroxyapatite coatings. *Biomaterials* **2005**, 26 (32), 6288-6295.

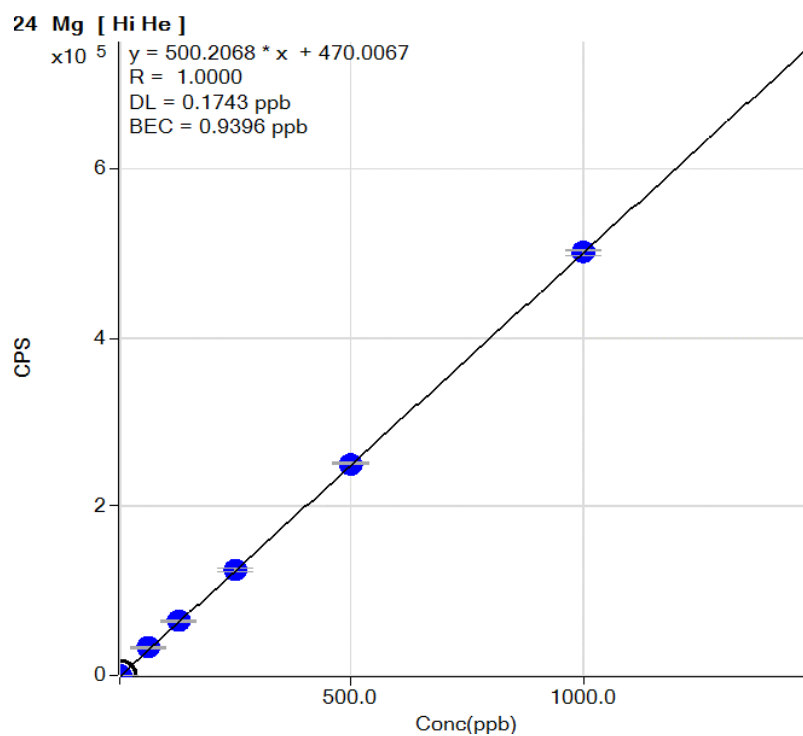
51. Fahami, A., Beall, G. W., Betancourt, T., Synthesis, bioactivity and zeta potential investigations of chlorine and fluorine substituted hydroxyapatite. *Materials Science & Engineering C-Materials for Biological Applications* **2016**, *59*, 78-85.
52. Smeets, R., Kolk, A., Gerressen, M., Driemel, O., Maciejewski, O., Hermanns-Sachweh, B., Riediger, D., Stein, J. M., A new biphasic osteoinductive calcium composite material with a negative Zeta potential for bone augmentation. *Head & Face Medicine* **2009**, *5* (1), 13.
53. Fahami, A., Beall, G. W., Mechano-synthesis of carbonate doped chlorapatite–ZnO nanocomposite with negative zeta potential. *Ceramics International* **2015**, *41* (9), 12323-12330.
54. Fournier, V., Marcus, P., Olefjord, I., Oxidation of magnesium. *Surface and Interface Analysis* **2002**, *34* (1), 494-497.
55. Mayer, I., Schlam, R., Featherstone, J., Magnesium-containing carbonate apatites. *Journal of Inorganic Biochemistry* **1997**, *66* (1), 1-6.
56. Wang, J., Chao, Y., Wan, Q., Zhu, Z., Yu, H., Fluoridated hydroxyapatite coatings on titanium obtained by electrochemical deposition. *Acta Biomaterialia* **2009**, *5* (5), 1798-1807.
57. Chen, K., Xie, K., Long, Q., Deng, L., Fu, Z., Xiao, H., Xie, L., Fabrication of core-shell Ag@ pDA@ HAp nanoparticles with the ability for controlled release of Ag⁺ and superior hemocompatibility. *RSC Advances* **2017**, *7* (47), 29368-29377.
58. Kačiulis, S., Mattogno, G., Pandolfi, L., Cavalli, M., Gnappi, G., Montenero, A., XPS study of apatite-based coatings prepared by sol–gel technique. *Applied Surface Science* **1999**, *151* (1-2), 1-5.
59. Khairallah, F., Glisenti, A., XPS study of MgO nanopowders obtained by different preparation procedures. *Surface Science Spectra* **2006**, *13* (1), 58-71.
60. Sivaranjini, B., Mangaiyarkarasi, R., Ganesh, V., Umadevi, S., Vertical Alignment of Liquid Crystals Over a Functionalized Flexible Substrate. *Scientific reports* **2018**, *8* (1), 8891.

Appendix

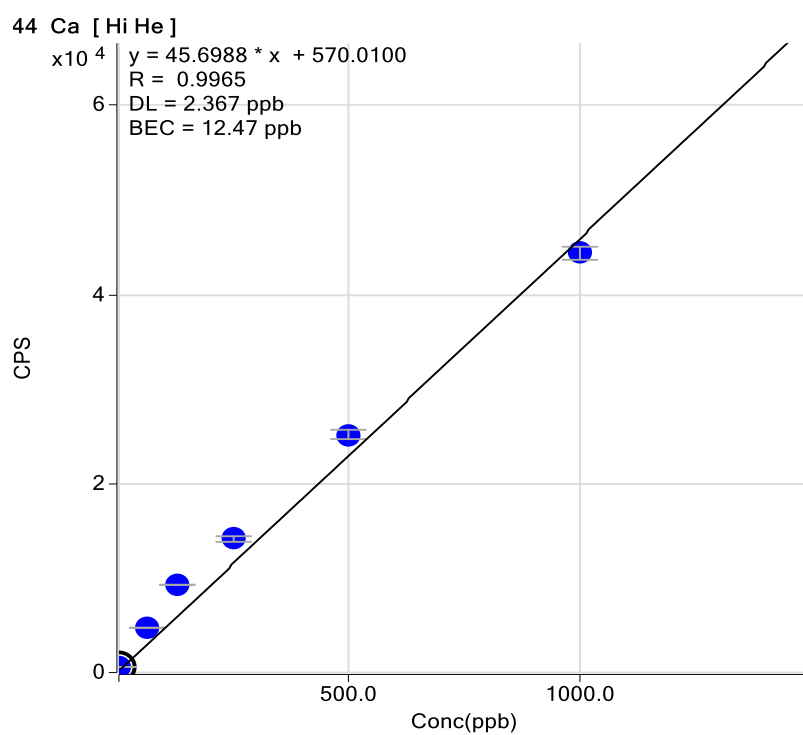


A.1 ICP calibration curve of (a) magnesium, (b) calcium and (c) phosphorus

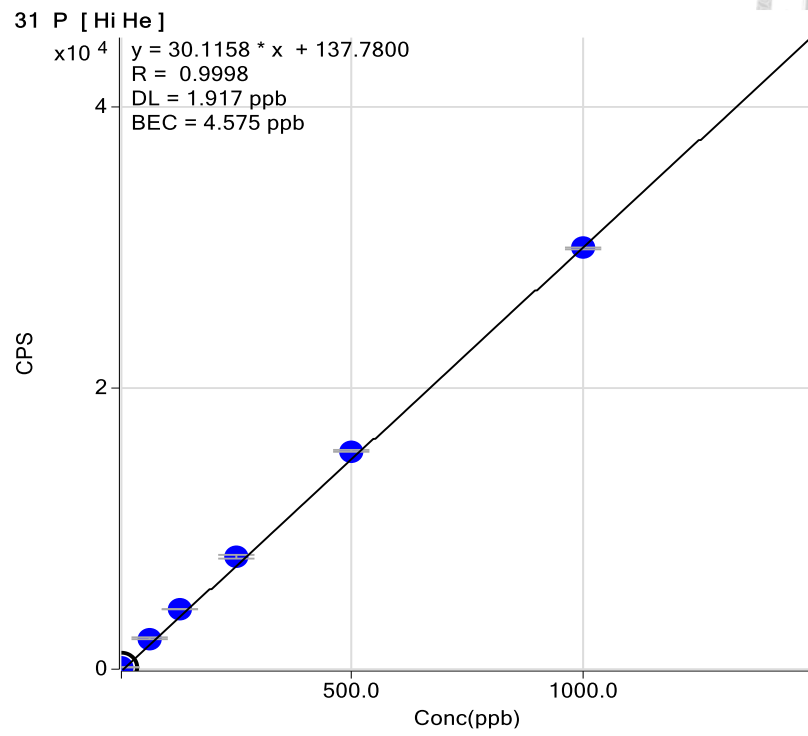
(a)



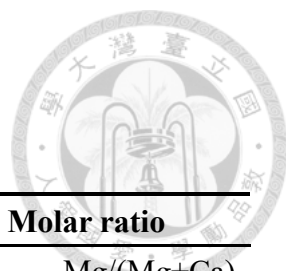
(b)



(c)



A.2 EDS of Mg@HAp and Mg@HAp-PC



Sample	Atom (%)			Molar ratio	
	Mg	Ca	P	Ca/Mg	Mg/(Mg+Ca) (%)
HAp (Ca/Mg=10)	1.03	63.66	35.31	61.81	1.59
HAp-PC (Ca/Mg=10)	3.50	60.34	36.16	17.24	5.48
HAp (Ca/Mg=5)	3.25	58.49	38.26	18.00	5.26
HAp-PC (Ca/Mg=5)	5.09	61.00	33.91	11.98	7.70
HAp (Ca/Mg=1)	12.43	52.35	35.22	4.21	19.19
HAp-PC (Ca/Mg=1)	39.30	12.39	48.31	0.32	76.03

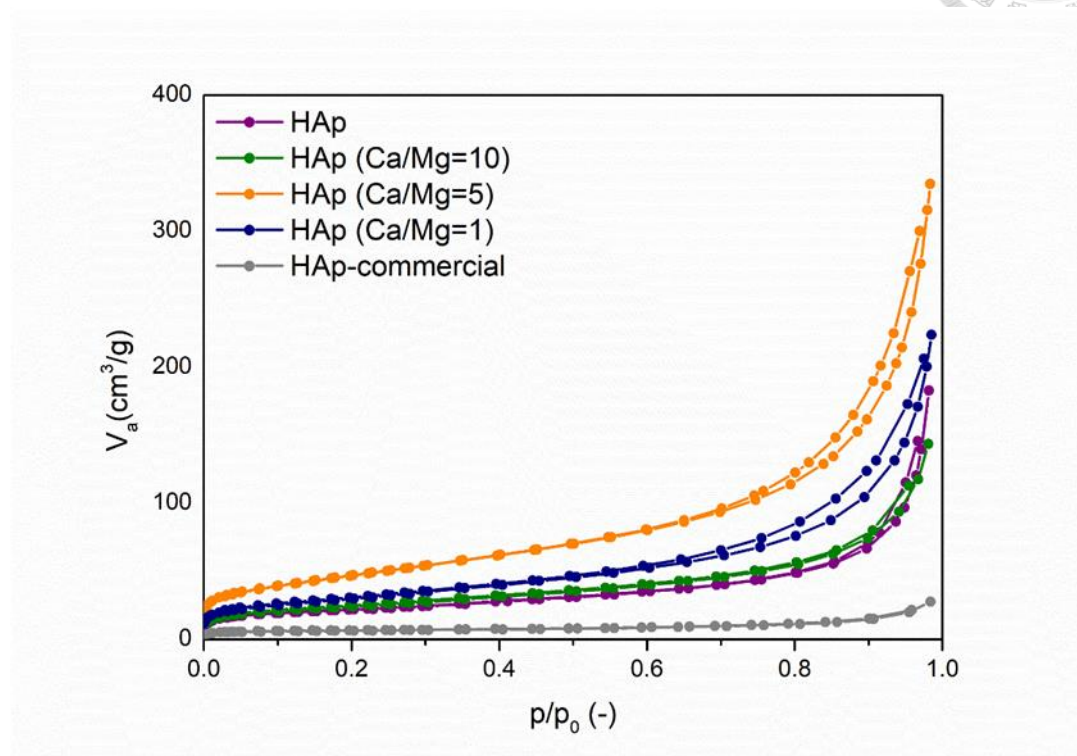
A.3 The specific surface area of Mg@HAp and Mg@HAp-PC

Material	Specific surface area (m ² /g)
Commercial HAp	22
HAp	77
HAp (Ca/Mg=10)	82
HAp (Ca/Mg=5)	155
HAp (Ca/Mg=1)	98
HAp-PC	22
HAp-PC (Ca/Mg=10)	30
HAp-PC (Ca/Mg=5)	46
HAp-PC (Ca/Mg=1)	14

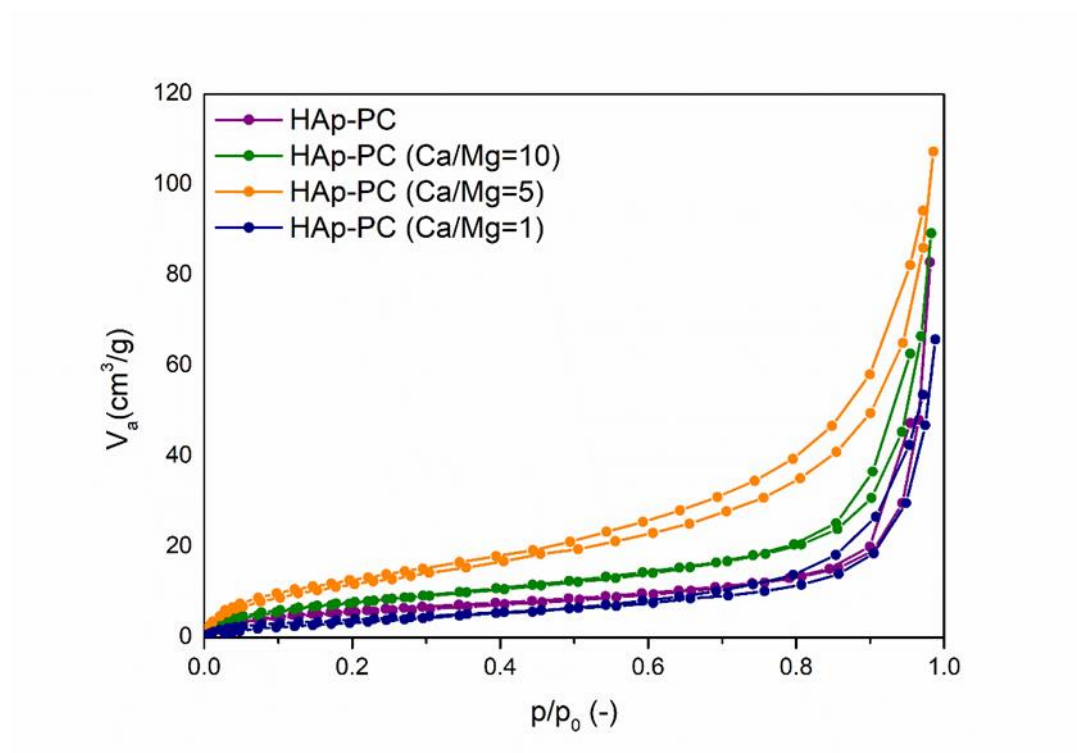


A.4 Adsorption and desorption isotherms of (a) Mg@HAp and (b) Mg@HAp-PC

(a)



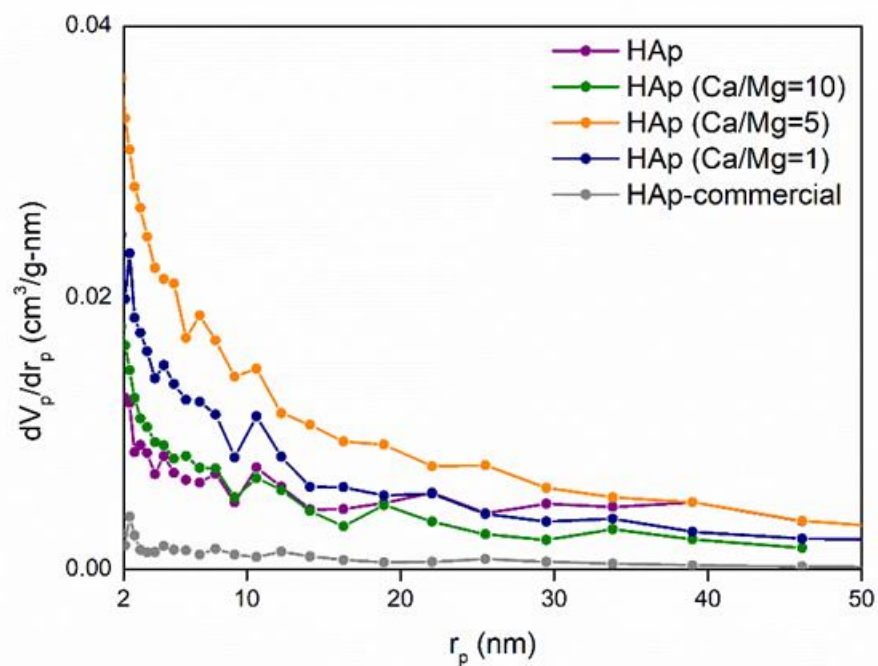
(b)



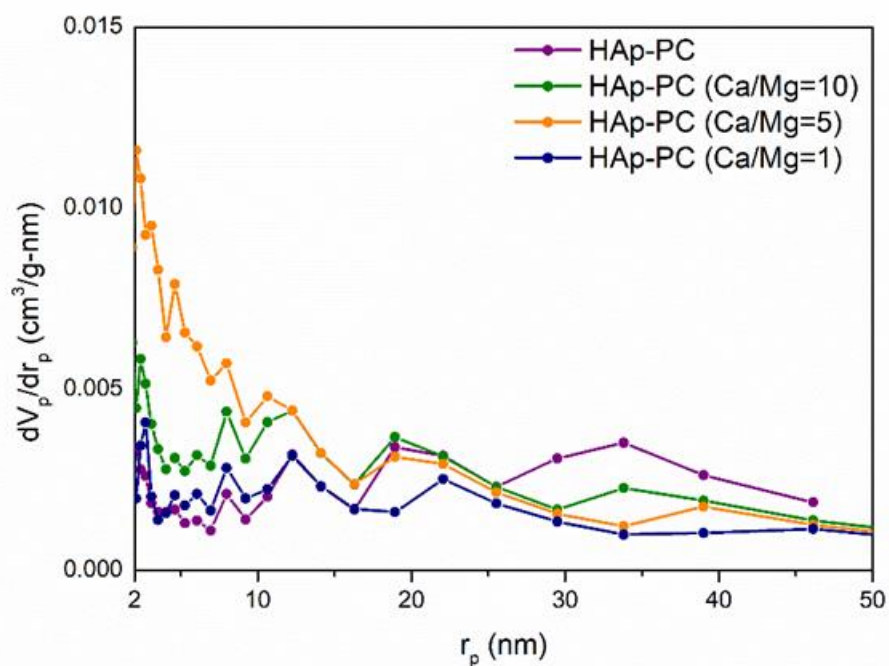


A.5 The mesoporous pore distribution of (a) Mg@HAp and (b) Mg@HAp-PC

(a)



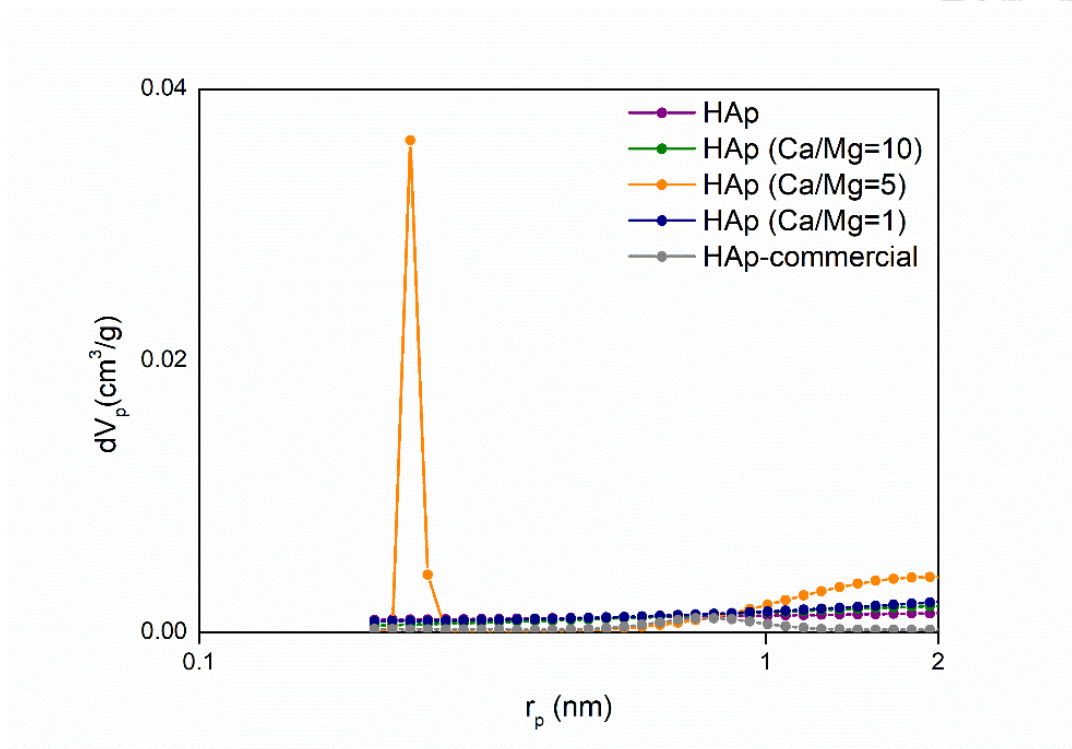
(b)



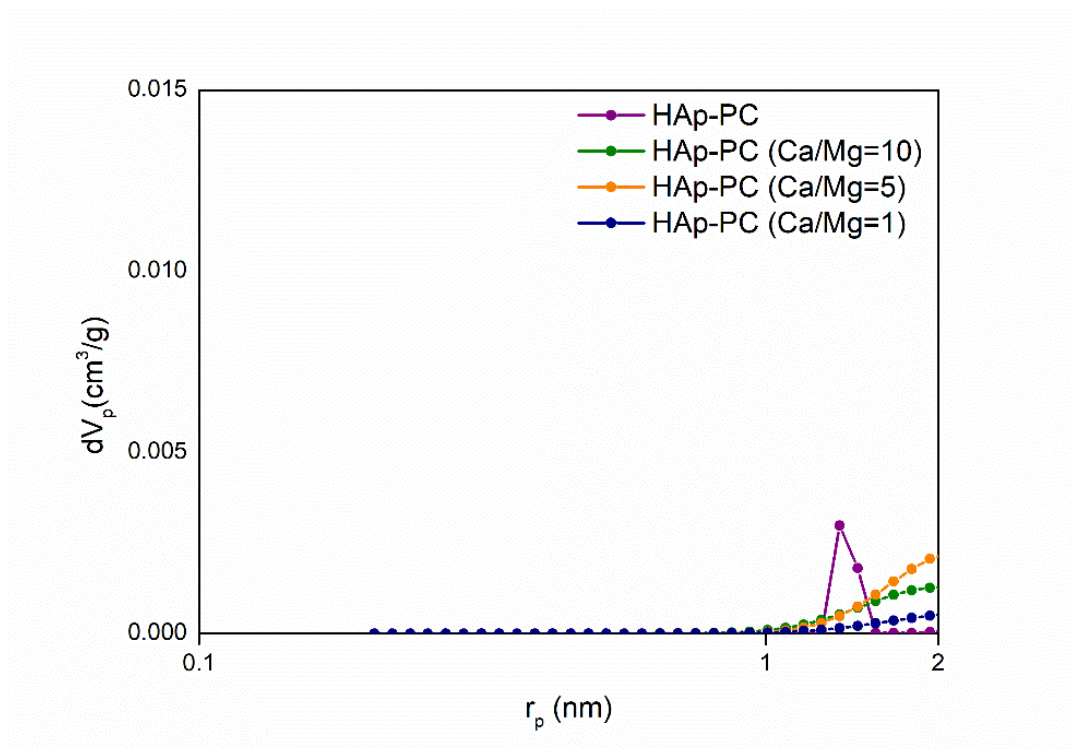


A.6 The microporous pore distribution of (a) Mg@HAp and (b) Mg@HAp-PC

(a)

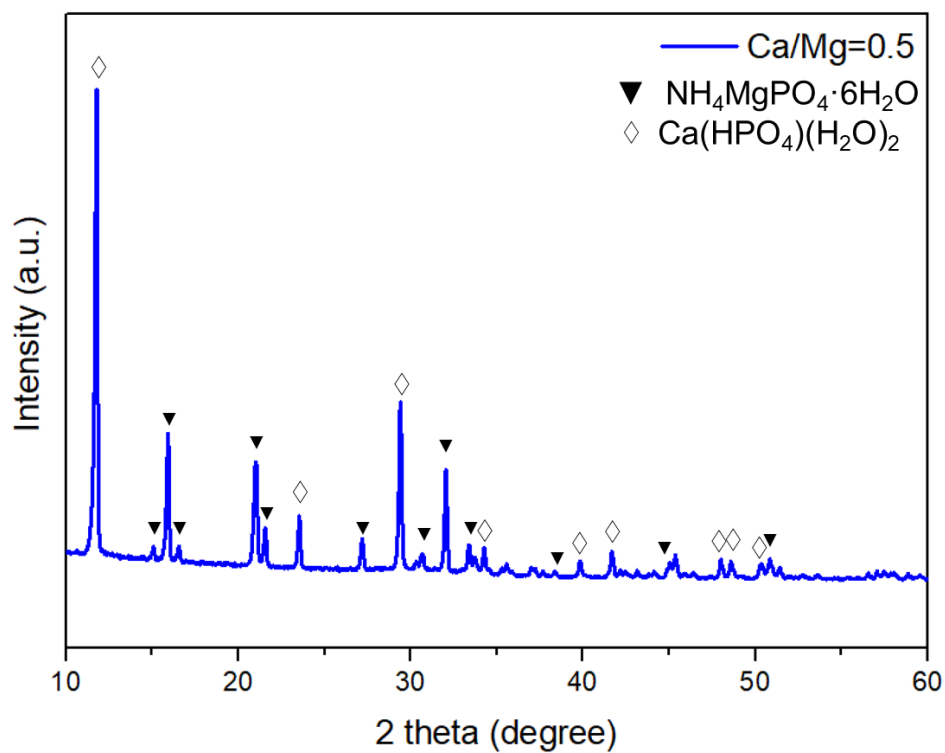


(b)

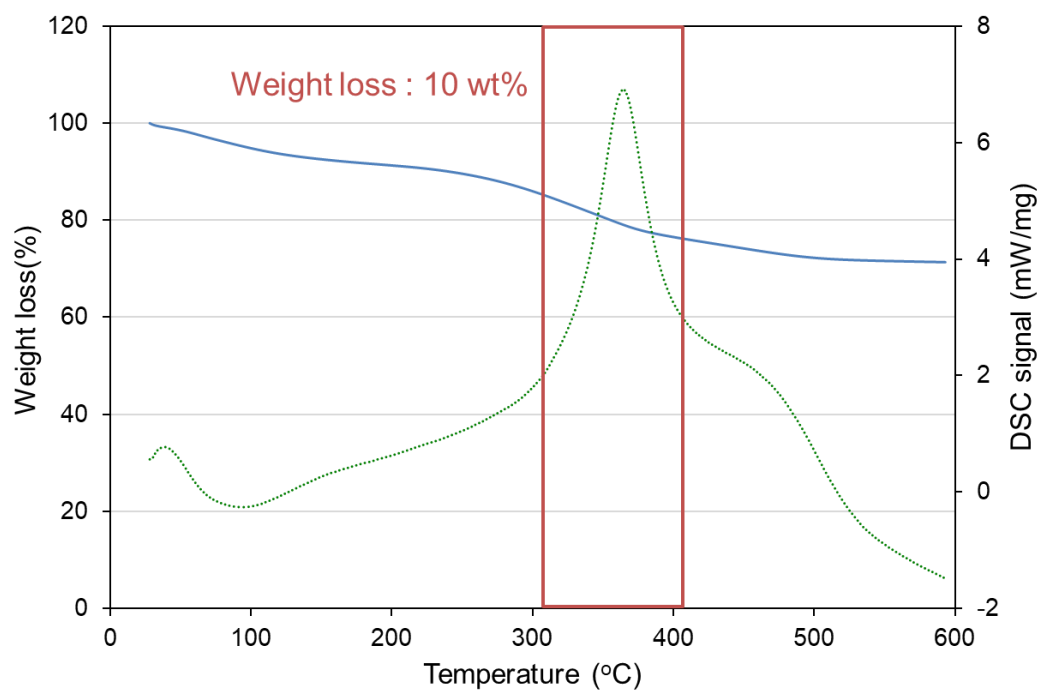





A.7 The XRD pattern of HAp (Ca/Mg=0.5)



A.8 TGA analysis of HAp-PC (Ca/Mg=5)



A.9 Hydrodynamic size of Mg@HAp and Mg@HAp-PC



Material	Hydrodynamic size (d. nm)
HAp	2458 ± 127
HAp-PC	2737 ± 944
HAp (Ca/Mg=10)	2920 ± 747
HAp-PC (Ca/Mg=10)	1406 ± 311
HAp (Ca/Mg=5)	3314 ± 274
HAp-PC (Ca/Mg=5)	988 ± 393
HAp (Ca/Mg=1)	1392 ± 57
HAp-PC (Ca/Mg=1)	1607 ± 846